Geoscience Frontiers 15 (2024) 101814

Contents lists available at ScienceDirect

Geoscience Frontiers

journal homepage: www.elsevier.com/locate/gsf

Research Paper

A new tectonic model for the Itmurundy Zone, central Kazakhstan: linking ocean plate stratigraphy, timing of accretion and subduction polarity

Inna Safonova [a,b], Ilya Savinskiy [c], Alina Perfilova [b,c,*], Olga Obut [d], Alexandra Gurova [b,c], Sergei Krivonogov [a,b]

[a] Southwest Jiaotong University, Xi'an Road 999, Chengdu, China
[b] Sobolev Institute of Geology and Mineralogy, SB RAS, Koptyuga Ave. 3, Novosibirsk, Russia
[c] Novosibirsk State University, Pirogova St. 2, Novosibirsk, Russia
[d] Trofimuk Institute of Petroleum Geology and Geophysics SB RAS, Koptyuga Ave. 3, Novosibirsk, Russia

ARTICLE INFO

Article history:
Received 1 December 2023
Revised 25 January 2024
Accepted 19 February 2024
Available online 23 February 2024
Handling Editor: M. Santosh

Keywords:
Central Asian Orogenic Belt
Accretionary complex
Magmatic rocks
Sedimentary rocks
Subduction polarity
Lithospheric plates

ABSTRACT

The Itmurundy Zone of Central Kazakhstan is a key structure in the core of the Kazakh Orocline representing a typical Pacific-type orogenic belt hosting accretionary complex, ophiolite massifs and serpentinite mélange. The main controversies in the existing tectonic models of the Itmurundy Zone are about the timing of subduction and accretion, the direction and kinematics of subduction and the number of oceanic plates. A new model for the early Paleozoic tectonic story of the Itmurundy Zone is postulated in this paper, based on new detailed geological and U–Pb detrital zircon age data, combined with previously documented geological, U–Pb age, microfossil, geochemical and isotope data from igneous rocks, deep-sea sediments and greywacke sandstones. The present study employs the Ocean Plate Stratigraphy (OPS) model to explain the tectonic processes involved in the evolution of the Itmurundy Zone and to present a holistic story of Ordovician oceanic plate(s), which accretion formed an accretionary complex. The detailed mapping allows distinguishing three types of OPS assemblages: (1) Chert-dominated, (2) OIB-hosting, and (3) MORB-hosting. The U–Pb ages of detrital zircons from sandstones of OIB and Chert types show unimodal distributions with similar main peaks of magmatism at 460–455 Ma in the provenance, and their maximum depositional ages (MDA) span 455–433 Ma. Two samples from OPS Type 3 show the peaks of magmatism both at ca. 460 Ma and the MDA of 452 Ma and 459 Ma, respectively. The MDA of sandstones and microfossils data from chert show the younging of strata to the south and SE in Types 1 and 2 and to NEE for Type 3 (in present coordinates) suggesting double-sided subduction to the NNW and SEE and, accordingly, the co-existence of pieces of two oceanic plates in Ordovician time. The U–Pb zircon data from both igneous and clastic rocks indicate a period of subduction erosion in early Ordovician time. As a whole, the accreted OPS units of the Itmurundy Zone record the timing of subduction and accretion from the early Ordovician to the early Silurian, i.e., 60 Ma at shortest.

1. Introduction

Reconstruction of paleo-oceans through study of accretionary complexes is a powerful approach providing evidence for the size, ages and direction of subduction (subduction polarity) of ancient oceanic plates and thus giving robust information about this or that stage of the Wilson cycle. Subsequent arriving of different segments of an oceanic plate, from the oldest to the youngest, to the subduction zone and their subsequent accretion allows us to reconstruct a story of an ancient oceanic plate from its birth at mid-oceanic ridge to its demise in the subduction zone using the model of ocean plate stratigraphy or OPS (Fig. 1A). The OPS is a regular succession of igneous and sedimentary rocks of the oceanic lithosphere, which were, respectively, erupted and deposited on the sea floor as the underlying oceanic basement traveled from mid-oceanic ridge to subduction zone (e.g., Isozaki et al., 1990; Matsuda and Isozaki, 1991; Wakita and Metcalfe, 2005; Safonova, 2009; Maruyama et al., 2010; Kusky et al., 2013; Safonova et al., 2016). The stable succession of OPS rocks from

* Corresponding author.
E-mail address: alinaperfilova@igm.nsc.ru (A. Perfilova).

https://doi.org/10.1016/j.gsf.2024.101814

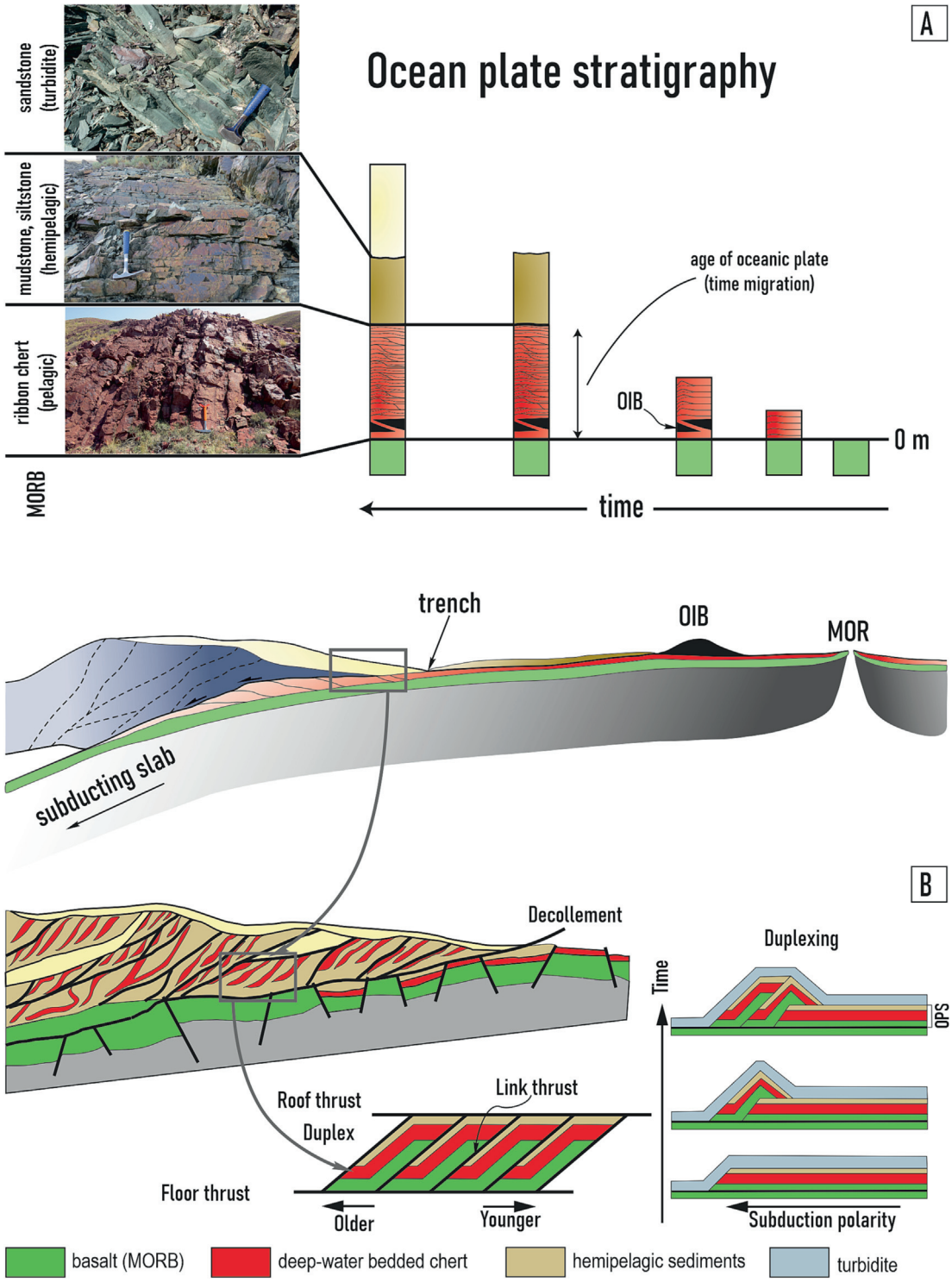

Fig. 1. A model of ocean plate stratigraphy, OPS. (A) A typical succession of deposition and eruption of OPS sedimentary and magmatic units, respectively, and their incorporation into accretionary complex (adapted from Isozaki et al., 1990; Safonova et al., 2020). (B) OPS packages or "horses" arriving to the subduction zone and accreted at different time to form duplexes; the cartoon also shows the faulted surface of the subducting slab forming a system of grabens and horsts (adapted from Safonova and Maruyama, 2014).

ocean floor basalt to pelagic chert, hemipelagic siliceous sediments (siliceous mudstone, siltstone, shale) and, finally, trench turbidite allows us to define subduction polarities of ancient oceanic plates even in such complicated structures as accretionary prism (Fig. 1B).

Oceanic sediments, while approaching an accretionary prism, can be thrust under older layers to form duplex structures consisting of OPS packages (horses) of different ages. In such horses the oldest OPS packages typically occur on the top and the youngest occur at the bottom part of the section (Fig. 1B) thus making the "traditional" identification of stratigraphic tops and bottoms impossible. Keeping in mind the stable succession of OPS lithologies (Fig. 1A) we can reconstruct subduction polarity and understand accretion mechanisms. For achieving this, we need to employ detailed in-field geological mapping with careful identifi-

cation of contacts between different lithologies and further estimation of the age of at least 2–3 OPS packages. During the last 30 years, a great progress has been achieved in the determination of the age of oceanic sediments using microfossils, typically radiolarians and conodonts (e.g., Kemkin and Khanchuk, 1994; Zyabrev and Matsuoka, 1999; Hori and Wakita, 2004; Wakita and Metcalfe, 2005; Tolmacheva et al., 2009). Although this method works well in Mesozoic and younger accretionary prisms and complexes of the western Pacific, it appears much less efficient in old orogenic belts formed in place of paleo-oceans because of the high degree of deformation, that destroys microfossils, induced by accretion, ocean suturing and further collision of continents. In that case, U–Pb dating of detrital zircons from clastic rocks, mainly from sandstones, can help. The study of U–Pb dating of detrital zircons from greywacke sandstones hosted by accretionary complexes has been becoming a more popular instrument for such reconstructions (e.g., Long et al., 2012; Jiang et al., 2017; Knittel et al., 2020; Lu et al., 2020; Safonova and Perfilova, 2023).

The Phanerozoic geological history of Asia is closely linked with the evolution of the Paleo-Asian Ocean (PAO), which suturing and closure formed the Central Asian Orogenic Belt (CAOB), the world largest accretionary intracontinental orogen extended from Kazakhstan and Uzbekistan in the west to eastern Russia and China (Fig. 2) (e.g., Zonenshain et al., 1990; Sengör et al., 1993; Buslov et al., 2001; Kovalenko et al., 2004; Windley et al., 2007; Yarmolyuk et al., 2012; Kröner et al., 2014; Safonova, 2017). The PAO opened in the late Neoproterozoic as a result of the breakup of the Rodinia supercontinent and was evolving, according to different evaluations, until the early Carboniferous or even the Triassic (e.g., Dobretsov et al., 1995; Li, 2006; Xiao et al., 2010, 2017; Eizenhöfer et al., 2014; Safonova et al., 2017). During the whole Paleozoic, numerous fragments of the oceanic crust and island arc were accreting to the Pacific-type convergent margins of the PAO.

In this paper, we present results of a seven-year multidisciplinary research program in the Itmurundy Zone of Central Kazakhstan in the western CAOB (Fig. 2). Our research included detailed geological mapping at seven sites (Fig. 3), U–Pb zircon dating of igneous and clastic rocks, micropaleontological study of deep-sea oceanic sediments, geochemical and whole-rock Nd and Hf-in-zircon isotope studies of igneous rocks and greywacke sandstones (Safonova et al., 2019, 2020, 2022; Perfilova et al., 2022). Based on our original data, both published and new, plus literature data we attempted to reconstruct OPS successions, subduction polarity and mechanisms of accretion at early Paleozoic Pacific-type convergent margins of the western Paleo-Asian Ocean.

2. Regional tectonic overview

The Itmurundy Zone of Central Kazakhstan is a part of the Paleozoides of Kazakhstan (e.g., Heinhorst et al., 2000; Yakubchuk,

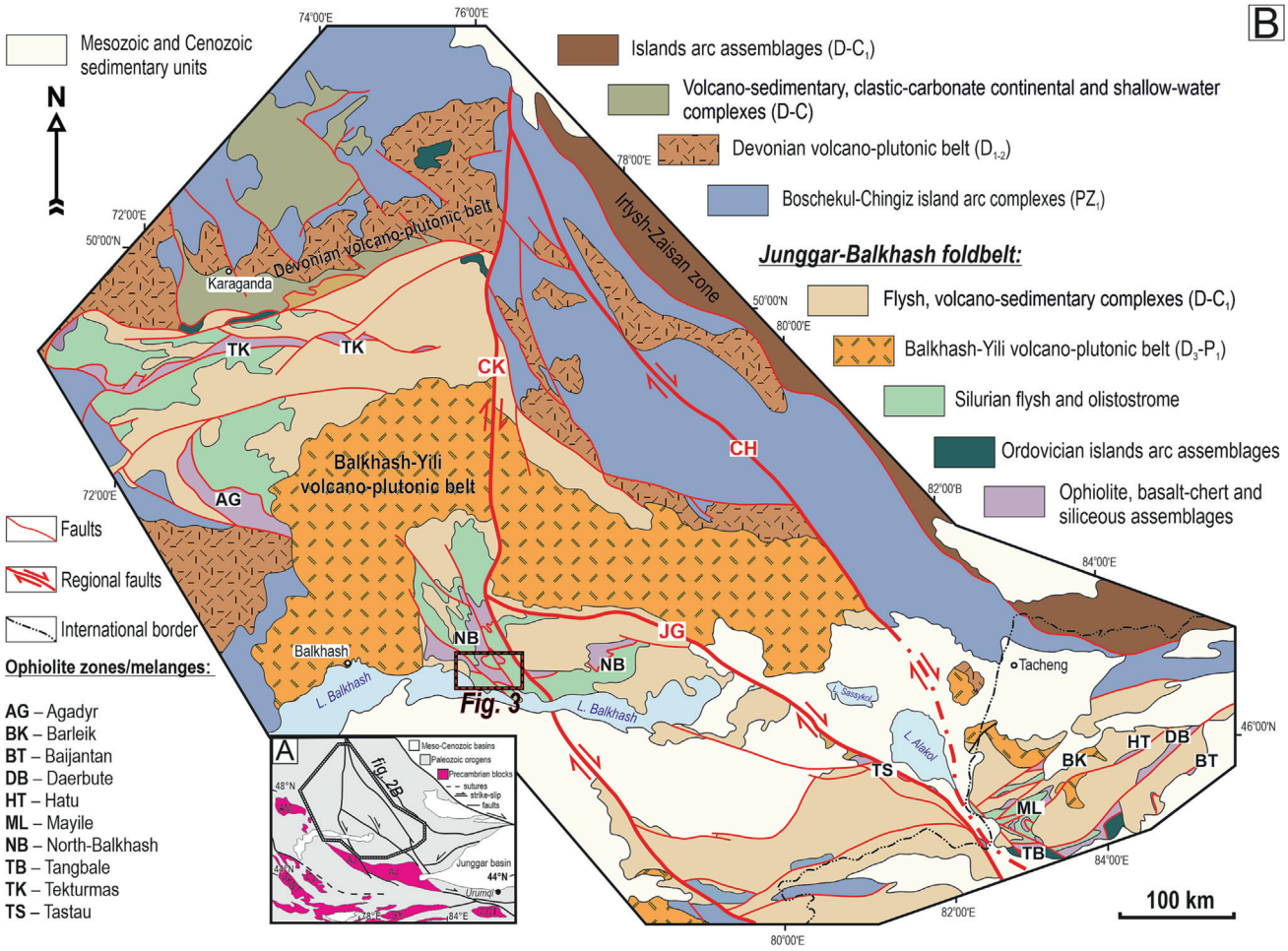

Fig. 2. (A) Sketch map of the southwestern part of the CAOB showing the distribution of main continental blocks and accretionary belts (modified from Windley et al., 2007; Wang et al., 2008, 2012; Alexeiev et al., 2011; Choulet et al., 2011). Microcontinents: AJ = Aktau-Junngar, AM = Aktau-Mointy, CCT = Chinese Central Tianshan, CY = Chu-Yili, SKNT = Stepnyak–Kyrgyz North Tian Shan, SY = South Yili. (B) Tectonic scheme of the north-western CAOB (modified from Degtyarev, 1999; Degtyarev et al., 2020; Perfilova, 2023). Regional faults: CK – Central Kazakhstan; CH – Chingiz; JG – Junggar.

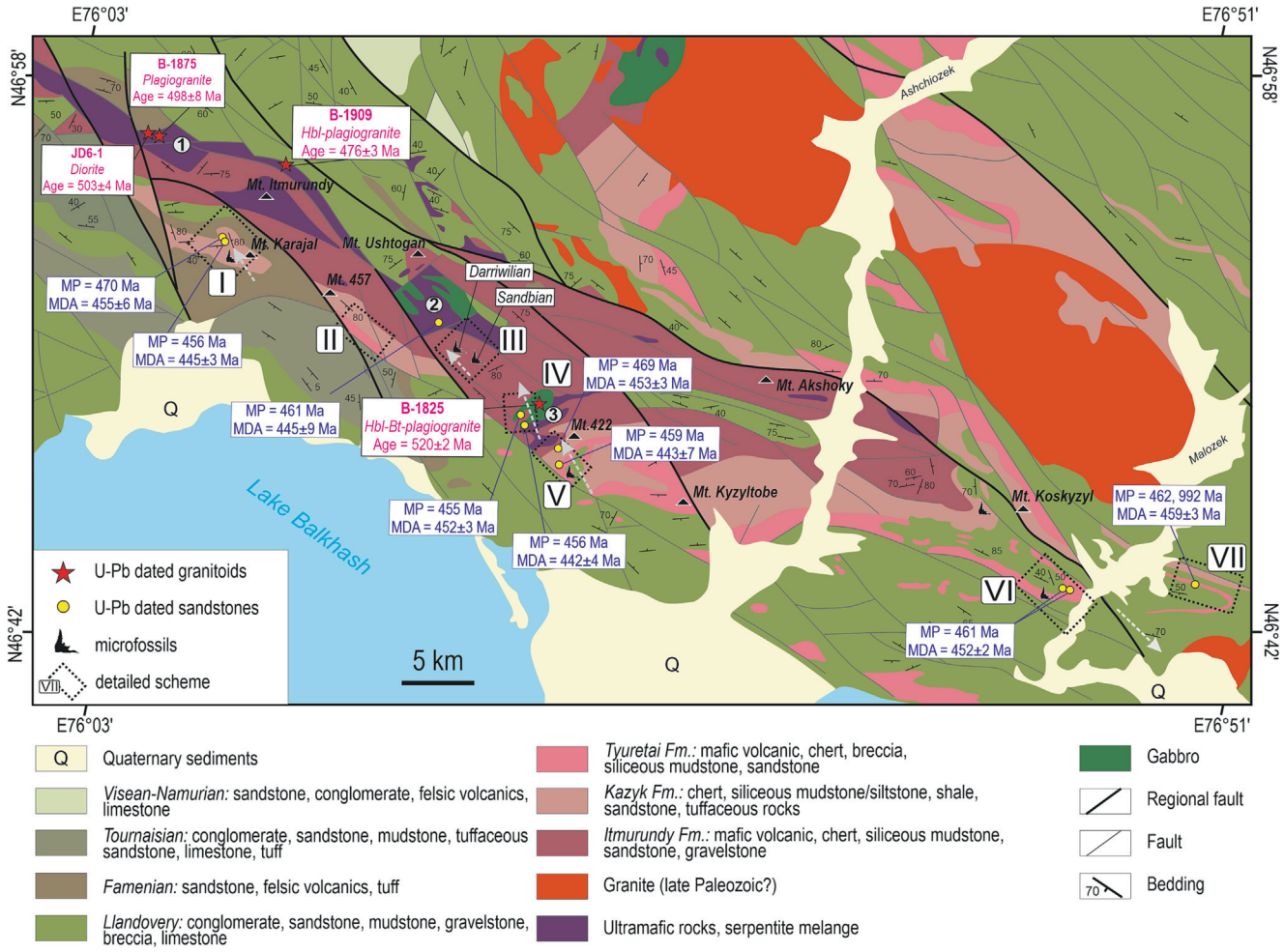

Fig. 3. The geological structure of the Itmurundy Zone modified from (Koshkin and Galitsky, 1960; Patalakha and Belyi, 1981). The stratigraphic subdivision is given as "initial" formation (see section 3.2). The light-grey dashed arrows show the proposed direction of subduction. U–Pb detrital zircon ages: MP – main peak(s), MDA – maximum depositional age. I-VII, sites of detailed mapping and sampling shown in Figs. 12, 14, 15. The numbers in circles are for the mafic–ultramafic massifs: 1, Kentarlau; 2, Arkharsu; 3, East Arkharsu.

2004; Degtyarev and Ryazantsev, 2007; Degtyarev, 2011, 2012; Korobkin, 2011), that is structurally posed in the core of the Kazakh Orocline (Levashova et al., 2003, 2012; Bazhenov et al., 2012; Li et al., 2018a), a key tectonic structure of the western CAOB (Fig. 2). The main tectonic structures of the Kazakh Paleozoides formed during the late Neoproterozoic-Paleozoic evolution of the PAO, middle Paleozoic coring and amalgamation of the young Kazakhstan continent and collisions of the Kazakhstan-Siberian and Siberian-East European continents (Zonenshain et al., 1990; Sengör et al., 1993; Berzin and Dobretsov, 1994; Didenko et al., 1994; Puchkov, 2000; Filippova et al., 2001; Windley et al., 2007; Xiao et al., 2009; Degtyarev, 2011). The Kazakh Paleozoides are bounded by the Ural-South Tienshan foldbelt from west and south-west and by the Junggar-Balkhash folded area from the south and south-east (Fig. 2). The Junggar-Balkhash folded area is, in turn, bounded by the Devonian volcanic belt and includes Silurian-early Devonian thick flysch and volcanogenic-clastic formations, which overlap Cambrian-Ordovician supra-subduction formations and middle Ordovician-early Silurian oceanic plate formations exposed within the relatively narrow and extended Tekturmas, North-Balkhash and Agadyr foldbelts (e.g., Degtyarev, 1999; Degtyarev and Ryazantsev, 2007). The North-Balkhash foldbelt includes the Itmurundy Zone (Figs. 2 and 3) consisting of Cambrian to Silurian ophiolites, accreted OPS units and clastic formations (Patalakha and Belyi, 1981; Safonova et al., 2019). The formation of the Itmurundy Zone is linked to the early Paleozoic Pacific-type orogeny (e.g., Dewey and Bird, 1970; Maruyama et al., 2011; Maruyama and Safonova, 2019) at convergent margins of the PAO. The early Paleozoic subduction of one or more oceanic plates of the PAO possibly under the active margins of the Kokchetav, North Tienshan, Aktau-Mointy and Junggar microcontinents (e.g., Levashova et al., 2010; Yarmolyuk et al., 2013; Degtyarev et al., 2017; Safonova, 2017), formed several intra-oceanic and continental magmatic arcs and related accretionary prisms. The magmatic arcs were separated from the coeval accretionary prisms by fore-arc units and older accretionary prisms, but later, during the late Paleozoic suturing of the PAO and subsequent approaches and collisions of the Junggar Block and the young Kazakhstan Continent or Kazakhstan Collage System with the Siberian Continent (e.g., Buslov et al., 2001; Degtyarev and Ryazantsev, 2007; Windley et al., 2007; Buslov, 2011; Xiao and Santosh, 2014; Xiao et al., 2015), they became juxtaposed in Pacific-type orogenic belts.

The tectonic structure of Central Kazakhstan is dominated by island-arc and continental-arc terranes and accretionary complexes, all parts of the Kazakh Orocline (Fig. 2). The extended and well-exposed Boshchekul-Chingiz and Baidaulet-Akbastau island-arc terranes are of Mariana-type and Japan-type, respectively (e.g., Xiao et al., 2010; Degtyarev, 2011; Safonova et al., 2017). The Boshchekul-Chingiz arc consists of mafic to intermediate volcanic rocks and felsic granitoids of middle Cambrian and middle-

late Ordovician ages (Degtyarev, 2012). The Baidaulet-Akbastau arc is composed mainly of basaltic to andesibasaltic lavas of early-middle Ordovician age and granitoids of late Ordovician age. The basement of the arc is heterogeneous consisting of both mafic and sialic domains (Degtyarev, 2012). In addition, middle-late Cambrian and early-middle Ordovician igneous rocks occur as fragments/blocks in serpentinite mélanges of the Itmurundy and Tekturmas zones (Degtyarev et al., 2020, 2021a,b; Khassen et al., 2020; Safonova et al., 2020, 2022; Gurova et al., 2022). The huge Devonian volcanic belt was formed at an Andean-type active continental margin and initially it was relatively straight. Its Silurian-early Devonian volcaniclastic formations were deposited in the fore-arc trough basin (Degtyarev, 2012). The bending of the Devonian belt started in late Devonian time was continuing until the late Paleozoic to form what we call now "Kazakh Orocline". Evidence for this comes from both structural and paleomagnetic data (Grishin et al., 1997; Levashova et al., 2003; Abrajevitch et al., 2008; Li et al., 2018a).

Another significant element of the Kazakh Orocline is the Balkhash-Yili volcano-plutonic belt of late Devonian to early Permian age also formed at an active continental margin. Like the Devonian Belt, it has a horseshoe shape (Fig. 2). Both the Devonian and Balkhash-Yili belts are dominated by continental volcanic and volcanogenic-sedimentary complexes. The volcanogenic-sedimentary packages are brachiform folded with bedding at 30°–40°. Those complexes unconformably seat on early Paleozoic and Precambrian formations of the Aktau-Junggar microcontinent, which is composed of pre-Neoproterozoic high-grade metamorphosed volcanic and sedimentary rocks, Meso-Neoproterozoic carbonate and clastic sedimentary rocks and Neoproterozoic mafic to felsic intrusions (Fig. 2A) (e.g., Degtyarev, 2011; Wang et al., 2014a, b; Degtyarev et al., 2017). The Boshchekul-Chingiz arc terrane forms the northern limb of the Kazakh Orocline, while the Tekturmas and Itmurundy zones compose the northern and southern cores of the orocline, respectively, and are dominated by accretionary complexes hosting OPS assemblages of Ordovician age and serpentinite mélanges (Fig. 2B) (Safonova et al., 2019, 2020, 2022; Degtyarev et al., 2020; Khassen et al., 2020; Gurova et al., 2022).

3. Geology of the Itmurundy Zone

3.1. Main structures and lithologies

The NW–SE striking Itmurundy Zone is 5 to 15 km wide and about 250 km long (Fig. 3). It includes ophiolites, mafic lavas, deep-sea siliceous sediments, clastic sedimentary rocks and serpentinite mélange with blocks of igneous and metamorphic rocks (Patalakha and Belyi, 1981; Ermolov et al., 1990; Zhylkaidarov, 1998; Degtyarev, 1999; Stepanets, 2016; Safonova et al., 2019, 2020, 2022; Degtyarev et al., 2020, 2021a). The mafic lavas, deep-sea siliceous sediments, siliciclastic sedimentary rocks occur as tectonic sheets thrust under or over each other during the accretion and form an accretionary complex that is spatially juxtaposed with the ophiolite massifs, both broken by numerous faults of different scales and ages (Safonova et al., 2019). There are four systems of regional faults striking from east to west (az. 270°–290°), from WWN to east (az. 300°–310°), from north to south (az. 350°–10°) and from NE to SW (az. 60°–70°), and two large anticline faults (in the western part of the zone), which NW-striking axes are nearly parallel to the main regional faults (Fig. 3).

From a historical retrospective, the sedimentary rocks of the Itmurundy Zone initially were referred to as jaspers, quartzites, sandstones, conglomerates and shales and considered as structurally complicated and deformed Ordovician-Silurian deposits of unclear stratigraphic position and mutual relationships (Rusakov, 1933). Later, in the 1960–1970-ties the formations of the Itmurundy Zone were considered as parts of a Caledonian megasynclinorium (Bespalov, 1956; Koshkin and Galitsky, 1960; Trifonov, 1967; Esenov et al., 1972). In the 1980-ties, they separately identified a Cambrian olistostrome or a chaotic complex (mixtite) and an ophiolite association of mafic and ultramafic igneous rocks (Patalakha and Belyi, 1981; Koshkin et al., 1987). Since the 1990-ties, the Itmurundy Zone has been regarded as hosting an incomplete ophiolite association of unclear age (Cambrian?) and an accretionary complex of early Ordovician-early Silurian ages overlapped by a Silurian flysch (Degtyarev, 1999). The co-occurrence of island-arc igneous rocks, blueschists, eclogites and oceanic sedimentary and volcanic rocks allowed our group to consider the Itmurundy Zone a Pacific-type orogenic belt (Safonova, 2017) and proposed to discuss its formations in terms of Ocean Plate Stratigraphy (Safonova et al., 2019, 2020). Accordingly, we consider that the Itmurundy Zone consists of the accreted Ordovician to early Silurian oceanic floor basalts and oceanic sediments, which represent an accretionary complex (AC), Cambrian-early Ordovician ophiolite massifs, serpentinite mélanges, and early Silurian (Llandovery) clastic deposits (Fig. 3).

The Ordovician igneous and sedimentary rocks of the Itmurundy AC are ocean floor (MORB) and oceanic rise (OIB) basalts (Safonova et al., 2020; Degtyarev et al., 2021a), pelagic ribbon chert, hemipelagic siliceous sediments (mudstone, siltstone), trench turbidites and greywacke sandstones, i.e., formed in oceanic settings (Fig. 3). All these lithologies fit the OPS model (Fig. 1). The Itmurundy serpentinite mélange incorporates blocks of ophiolites: ultramafics (harzburgite, dunite, wherlite), gabbro, sheeted-dikes, and plagiogranites (Figs. 3 and 4). In addition, the mélange carries fragments of OPS rocks, both igneous and sedimentary, jadeitite, eclogite and glaucophane schists (Antonyuk, 1974; Patalakha and Belyi, 1981; Avdeev, 1986; Ermolov et al., 1990; Ermolov, 2008; Safonova et al., 2019, 2020; Degtyarev et al., 2021a). The ultramafic rocks are typically strongly altered to form lizardite, antigorite and chrysotile serpentinites.

3.2. Stratigraphy and micropaleontology

All the available stratigraphic subdivisions of the Itmurundy Zone have been distinguished based on micropaleontological data. The micropaleontological studies of Itmurundy deep-water siliceous sediments started as early as in the 1980-ties and are still continuing (Novikova et al., 1983; Koshkin et al., 1987; Zhylkaidarov, 1998; Nikitin, 2002; Safonova et al., 2019; Degtyarev et al., 2020). Most of the microfossil age constraints from the Itmurundy Zone are based on conodonts in reddish cherts and siliceous mudstones/tuffites. Initially only three formations were recognized in the study area (Figs. 3 and 4): Itmurundy (O_2), Kazyk ($O_{2\text{-}3}$) and Tyuretai (O_3-S_1) (Bespalov, 1956; Koshkin and Galitsky, 1960; Trifonov, 1967; Esenov et al., 1972; Patalakha and Belyi, 1981). Later they additionally distinguished four more formations: Ushbulak (O_2), Uzuntobek ($O_{2\text{-}3}$), Obaly (O_3) and Ashchiozek (S_1) (Koshkin et al., 1987; Zhylkaidarov, 1998; Nikitin, 2002; Degtyarev et al., 2020, 2021a).

The Itmurundy Fm. (O_2) is cropping out in the central part of the Itmurundy Zone (Fig. 3) and is dominated by OIB-type basalts, often pillowed, plus small outcrops of OIB-type andesibasalt and supra-subduction andesite having no clear contacts with surrounding rocks (Safonova et al., 2019, 2020; Perfilova et al., 2022). The basalts co-occur with ribbon chert, siliceous mudstones, siltstones and fine-grained sandstones. There are also beds of conglomerate, breccia and gravelstone (Figs. 4 and 5). The middle Ordovician age of the Itmurundy Fm. (Darriwilian) was constrained by conodonts (*Paroistodus horridus* and *Pygodus serra*) in the ribbon chert and

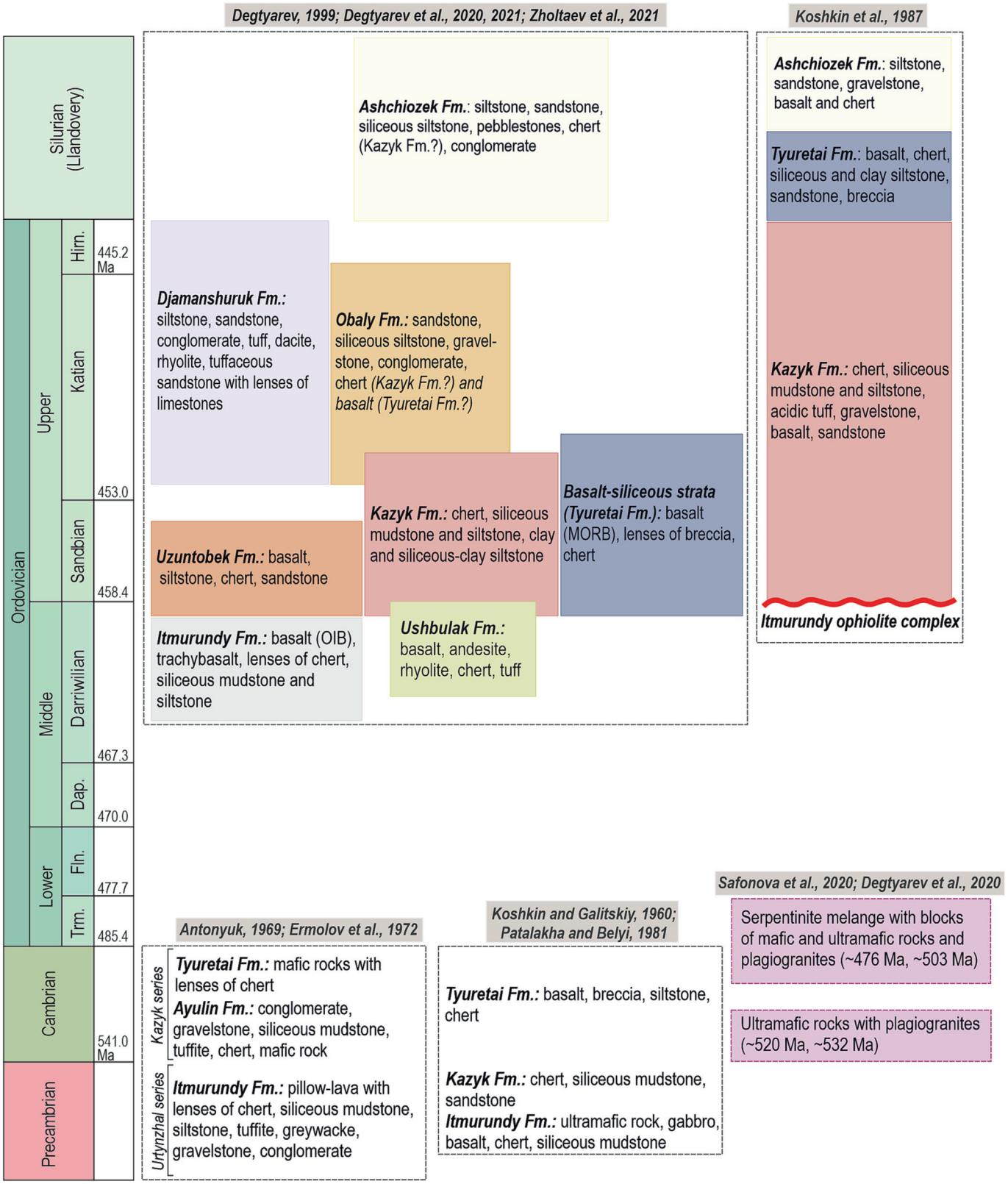

Fig. 4. Stratigraphic subdivisions of the Itmurundy Zone from a historical retrospective.

tuffaceous siltstone overlying the basalts (Novikova et al., 1983; Degtyarev et al., 2020). In general, the lithological composition of the Itmurundy Fm. is variable changing both vertically and laterally; the sedimentary packages often wedge out, boundinated and duplexed (see also Supplementary Data Figs. S1 and S2 for photos).

The Kazyk Fm. (O_{2-3}) is dominated by red and brown ribbon cherts, brown and grey-lily, chocolate siliceous mudstones and brown and grey-yellow siltstones (Figs. 5 and 6). The Kazyk sedimentary rocks are exposed in the western and central parts of the Itmurundy Zone (Fig. 3). The middle-late Ordovician age of the Kazyk Fm. (late Darriwilian to early Katian) is defined also by

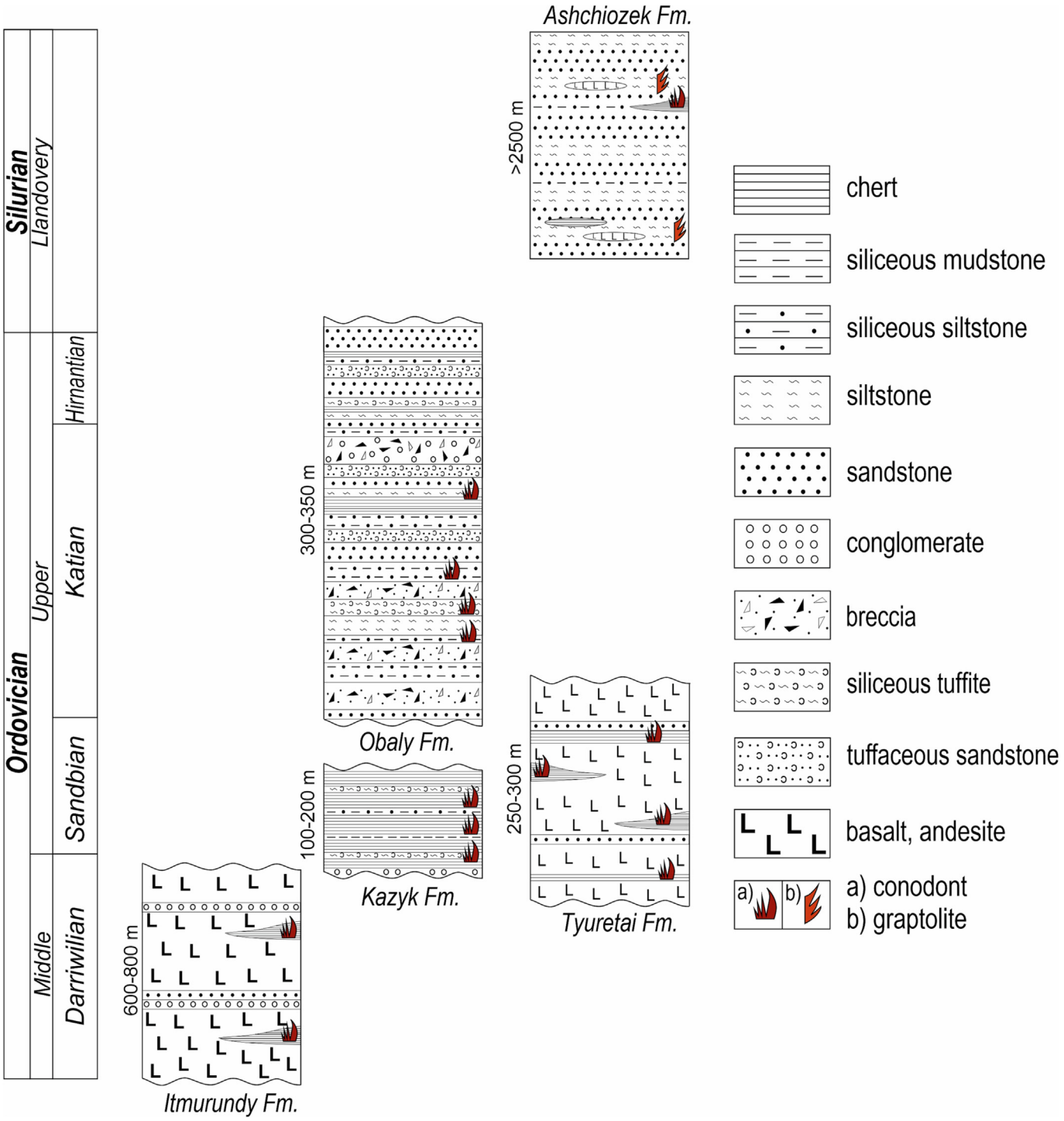

Fig. 5. Updated stratigraphic columns of the key formations of the Itmurundy Zone; the data on microfauna and U–Pb detrital zircon ages are from (Novikova et al., 1983; Koshkin et al., 1987; Zhylkaidarov, 1998; Nikitin, 2002; Safonova et al., 2019, 2022; Degtyarev et al., 2020; Perfilova et al., 2022).

conodonts (*Pygodus anserinus* and *Periodon grandis*) hosted by red ribbon chert (Figs. 5 and 6) (Novikova et al., 1983; Safonova et al., 2019; Degtyarev et al., 2020). Note that the conodont taxa that were fixed in the Kazyk Fm. are typical of deep-water facies and are widely distributed worldwide (Sweet and Bergstrom, 1984; Zhen and Percival, 2003; Tolmacheva et al., 2021). The rate of sedimentation of the Kazyk cherts is estimated as slow as 10 m per 1 Myr (Tolmacheva et al., 2004, 2021; Degtyarev et al., 2020).

The Tyuretai Fm. (O_3-S_1) is cropped out mainly in the eastern part of the Itmurundy Zone (Fig. 3). The Tyuretai deposits occur at the flanks of a large anticline structure. The Tyuretai Fm. is dominated by clastic sedimentary rocks (sandstone, gravelstone) and includes MORB-type basalts, siliceous mudstone and siltstone and breccia (Bespalov, 1956; Trifonov, 1967; Esenov et al., 1972; Patalakha and Belyi, 1981). The basalts are also often pillowed, amygdaloidal and brecciated; the porphyric varieties are less abundant and, in places, carry sparse beds of ribbon chert and lenses of

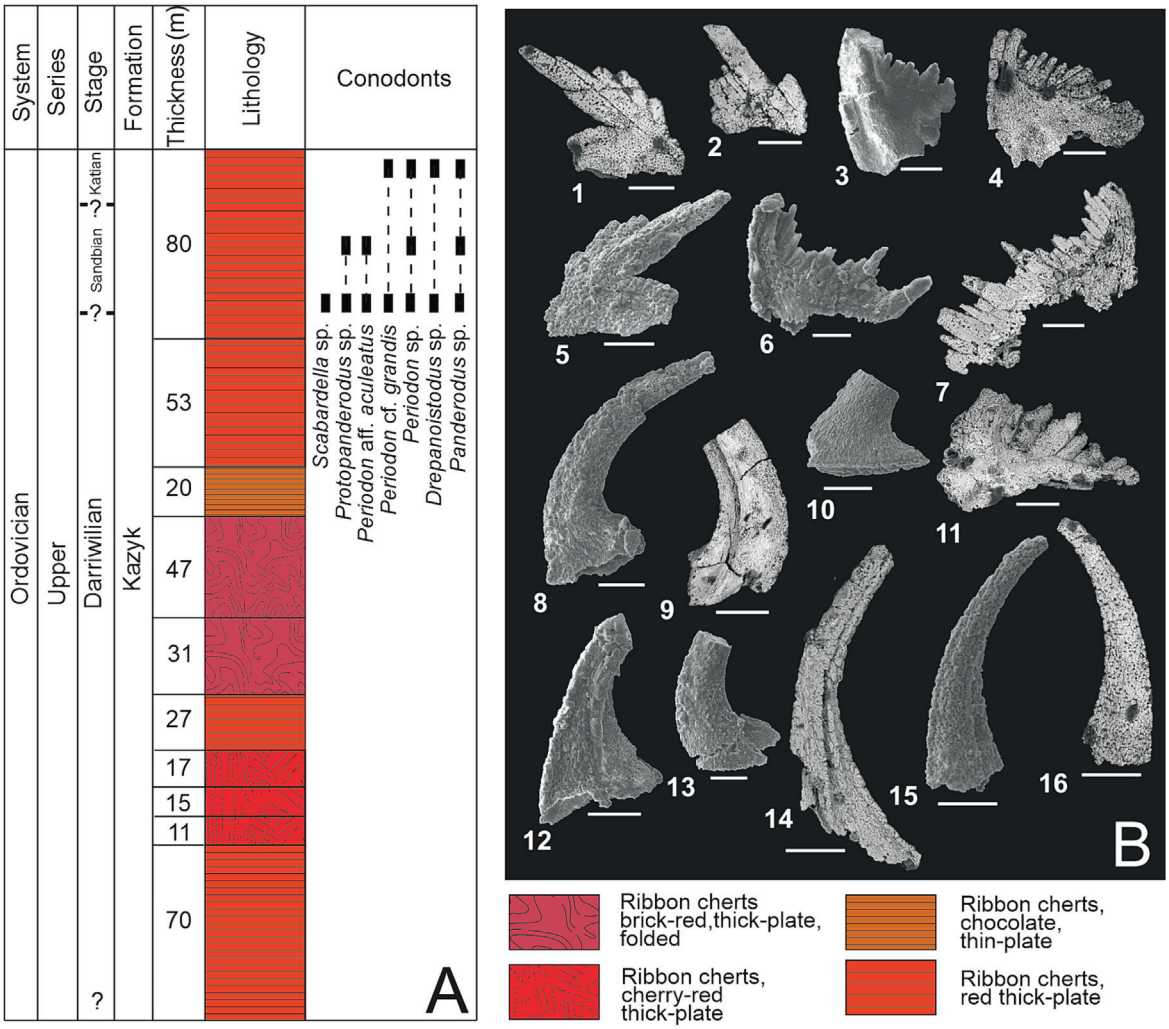

Fig. 6. Microfossils age constraints on the Kazyk Fm. (modified and expanded from Safonova et al., 2019). (A) Columnar section showing microfossil-based age ranges. (B) SEM photographs of conodonts from cherts of the Kazyk Fm.: 1, 2, 5 – Periodon cf. grandis (Ethington), 1, 5 – M elements, 2 – P element; 3, 4, 6, 7, 11 – Periodon sp., S elements; 8, 10 – Drepanoistodus sp., S elements; 9, 14 – Protopanderodus sp., S elements; 12 – Scabardella sp., S element; 13, 15, 16 – Panderodus sp. See also Table 1.

tuff (Degtyarev, 1999; Degtyarev et al., 2020; Safonova et al., 2020; Zholtaev et al., 2021). No direct contacts between the basalts, cherts and sandstones have been found due to poor exposure. The lenses/blocks of chert and MORB-type basalt are submerged into a siltstone-sandstone matrix of early Silurian age, which can be attributed to the Ashchiozek Fm. (Fig. 4; Degtyarev et al., 2021a). The middle-late Ordovician age of the Tyuretai Fm. (Darriwilian-Katian) was constrained by conodonts in cherts (*Pygodus anserinus* and *Periodon grandis*) (Novikova et al., 1983; Degtyarev et al., 2020). The early Silurian age of the clastic matrix was constrained by graptolites in siltstones (*Demirastrites triangulatus, Glyptograptus tamariscus vasians, G. nicolaevi)* (Table 1; Fig. 5) (Zhylkaidarov, 1998).

The Ushbulak Fm. (O_2) is dominated by volcanic rocks (basalt, andesite, rhyolite, tuffs of variable compositions) of supra-subduction origin (Degtyarev et al., 2021a). In addition, it includes sandstones and subordinate siliceous claystones and mudstones. Evidence for its middle Ordovician age comes from conodonts (*Periodon aculeatus* and *Drepanoistodus)* in the red claystones that occur in lenses in dacite (Degtyarev et al., 2020).

The Uzuntobek Fm. ($O_{2\text{-}3}$) is compositionally and chronologically similar to the Ushbulak Fm. It consists of pillow-lavas, siliceous tuffites and siltstones intercalated with red siliceous mudstones and cherts with lenses of sandstones and gravelstones. The tuffites contain middle-late Ordovician conodonts (*Pygodus anserinus* of the lower *Periodon grandis* biozone) (Degtyarev et al., 2020).

The Obaly Fm. (O_3) is dominated by siliciclastic sedimentary rocks: siliceous tuffites and siltstones, polymictic sandstones, gravelstones and conglomerates (Figs. 4 and 5). The siliceous tuffites and siltstones carry Sandbian-Hirnantian conodonts *Periodon grandis, Scabbardella altipes*, and *Drepanodus* sp. (Nikitin, 2002; Degtyarev et al., 2020). The coarse-grained clastic rocks carry fragments of red chert and chocolate siliceous siltstone similar to those of the Kazyk Fm.

The Ashchiozek Fm. (S_1) includes terrigenous/siliciclastic rocks and an olistostrome, both composing tectonic sheets that are thrust over the middle-late oceanic Ordovician formations (Degtyarev et al., 2020). The olistostrome consists of a clastic matrix (poorly sorted sandstones and siliceous siltstones) and olistoliths of basalt and chert. The basalts resemble those of the Tyuretai Fm. The cherts are visually similar to those of the Kazyk Fm. and contain upper Ordovician conodonts *Pygodus serra, Panderodus gracilis, Spinodus spinatus,* and *Periodon grandis* (Degtyarev et al., 2020). The siliceous siltstones carry Llandoverian graptolites, e.g., *Gliptograptus tamariscus, Coronograptus gregarious, Monoclimacis crenularia* and others (Koshkin et al., 1987) (for more details on the microfossils see Table 1).

Table 1
Microfossil data on conodonts from cherts of the Itmurundy accretionary complex.

№	Sites	Locality	Formation	Conodonts	Age	Reference
1	I	Mt. Karajal	Itmurundy	*Pygodus anserinus* Lamot et Lindstrom; *Periodon* cf. *grandis* (Ethington) Pygodus anserinus - Periodon grandis conodont zones	late Darriwilian–early Katian	Zhylkaidarov, 1998
2	II	Arkharsu	Itmurundy	*Periodon aculeatus* Hadding, *Drepanodus* cf. *arcuatus* Pander	middle Darriwilian–early Sandbian	Novikova et al., 1983
3	IV	Arkharsu	Itmurundy	*Periodon aculeatus* Hadding; *Pygodus serra* (Hadding); *Drepanodus* sp.Periodon aculeatus – Pygodus serra conodont zones	middle–late Darriwilian	Degtyarev et al., 2020
4	IV	Arkharsu	Uzuntobek (Itmurundy)	*Pygodus anserinus* Lamot et Lindstrom; *Periodon grandis* (Ethington); *Drepanodus* sp. Pygodus anserinus - Periodon grandis conodont zones	late Darriwilian–early Katian	Degtyarev et al., 2020
5	V	Mt. 422	Kazyk	*Periodon* aff. *aculeatus* Hadding; *Periodon* cf. *P. grandis* (Ethington); *Panderodus* sp.; *Drepanodus* sp. *Protopanderodus* sp., *Pygodus* sp.	late Darriwilian– early Katian	Safonova et al., 2019: new data
6	n.a.	Mt. Susyzkara	Kazyk	*Periodon* aff. *aculeatus* Hadding; *Pygodus* cf. *anserinus* Lamot et Lindstrom	late Darriwilian–early Sandbian	Novikova et al., 1983
7	n.a.	North of Ashchiozek Vil.	Tyuretai	*Pygodus serra* (Hadding); *Pygodus* cf. *anserinus* Lamot et Lindstrom; *Periodon aculeatus* Hadding	late Darriwilian–early Sandbian	Novikova et al., 1983
8	n.a.	8 km SW of Mt. Obaly	Itmurundy	*Periodon aculeatus* Hadding	middle Darriwilian–early Sandbian	Zhylkaidarov, 1998
9	n.a.	8 km SW of Mt. Obaly	Kazyk	*Pygodus anserinus* Lamot et Lindstrom Pygodus anserinus conodont zone	late Darriwilian	Zhylkaidarov, 1998
10	n.a.	Western Itmurundy Zone	Itmurundy	*Pragmodus* cf. *flexuosus* Moskalenko; *Cordylodus ramosus* Hadding; *Periodon aculeatus* Hadding; *Paroistodus originalis* (Sergeeva); *Protopanderodus rectus* Lindstrom	Dapingian–Darriwilian	Nikitin, 2002
11	n.a.	Western Itmurundy Zone	Kazyk	*Pygodus serra* (Hadding); *Pygodus anserinus* Lamot et Lindstrom	late Darriwilian–early Katian	Nikitin, 2002
12	n.a.	North Balkhash	Tyuretai	*Pygodus serra* (Hadding)	late Darriwilian	Nikitin, 2002
13	n.a.	3.5–4 km east of Mt. Obaly	Kazyk	*Pygodus anserinus* Lamot et Lindstrom; *Periodon grandis* (Ethington); *Scabbardella altipes* (Henningsmoen); *Spinodus spinatus* (Hadding); *Drepanodus* sp.; *Protopanderodus* sp. Pygodus anserinus - Periodon grandis conodont zones	late Darriwilian– early Katian	Degtyarev et al., 2020
14	n.a.	Mt. Tyuterai; 1 km south of Mt. Obaly	Tyuretai	*Periodon grandis* (Ethington); *Protopanderodus* sp.; *Scabbardella altipes* (Henningsmoen); *Per.* cf. *Per. aculeatus* Hadding Pygodus anserinus - Periodon grandis conodont zones	late Darriwilian–early Katian	Degtyarev et al., 2020

For details on the localities and ages see also Figs. 3, 4, 6-8.

All those "additional" formations, Ushbulak, Uzuntobek, Obaly and Ashchiozek (Fig. 4), are locally exposed and overlap by age and composition with the "initial" formations. As most of the geological boundaries between the formations are tectonic (Safonova et al., 2019, 2020), we think that the Ushbulak, Uzuntobek, Obaly and Ashchiozek formations can be partly or completely attributed to the better constrained Itmurundy or Kazyk or Tyuretai formations (Figs. 4 and 5). Such a situation with mapping is typical of many structurally complicated accretionary complexes hosted by fossil Pacific-type orogenic belts, like the CAOB (e.g., Dobretsov et al., 2004; Zhang et al., 2018; Dagva-Ochir et al., 2020; Khassen et al., 2020; Safonova et al., 2020; Savinskiy et al., 2021). The researchers of numerous younger accretionary complexes of the Western Pacific typically avoid using "traditional" stratigraphic subdivisions, but consider lithologically and chronologically different tectonic sheets as units (e.g., Khanchuk, 1993; Nakae, 2000; Wakita and Metcalfe, 2005; Kojima et al., 2008; Kusky et al., 2013; Wakita, 2013; Kemkin et al., 2016; Safonova et al., 2016). However, we are not ready yet to separate the study area into units, as each potential unit must be well constrained chronologically, either by microfossils or by U–Pb zircon ages, that remains challengeable. In this paper we consider the "initial" formations only: Itmurundy, Kazyk and Tyuretai.

3.3. U–Pb zircon age constraints

The first U–Pb zircon data from igneous rocks of the Itmurundy Zone have been obtained only three years ago: a supra-subduction hornblende diorite found as a block in the Kentaralau serpentinite mélange (Figs. 3 and 4) yielded a U–Pb age of 503 ± 4 Ma, i.e., middle Cambrian (Safonova et al., 2020). A bit later, there were reported several early Cambrian to Early Ordovician ages constrained also from supra-subduction granitoids: 531 ± 6 Ma and 532 ± 2 Ma from amphibole and biotite plagiogranites (Tesiktas Massif), 520 ± 2 Ma from plagiogranite (East Arkharsu Massif), 498 ± 8 Ma and 476 ± 6 Ma from amphibole plagiogranites present as blocks in serpentinite mélange (Kentaralau) (Degtyarev et al., 2021a; Supplementary Data Table S1). In recent papers (Perfilova et al., 2022; Safonova et al., 2022), we presented first U–Pb ages of detrital zircons from greywacke sandstones sampled in the central and eastern parts of the Itmurundy Zone (Fig. 3). In addition, in this paper we present first data from its western part (Figs. 7 and 8).

The sandstones from the central part (sites III-V in Fig. 3, near Karajal Mt.) are characterized by unimodal distributions of U–Pb detrital zircon ages with main peaks at 469 Ma, 461 Ma, 459 Ma, 456 Ma, 455 Ma, and 445 Ma, i.e., Middle-Late Ordovician

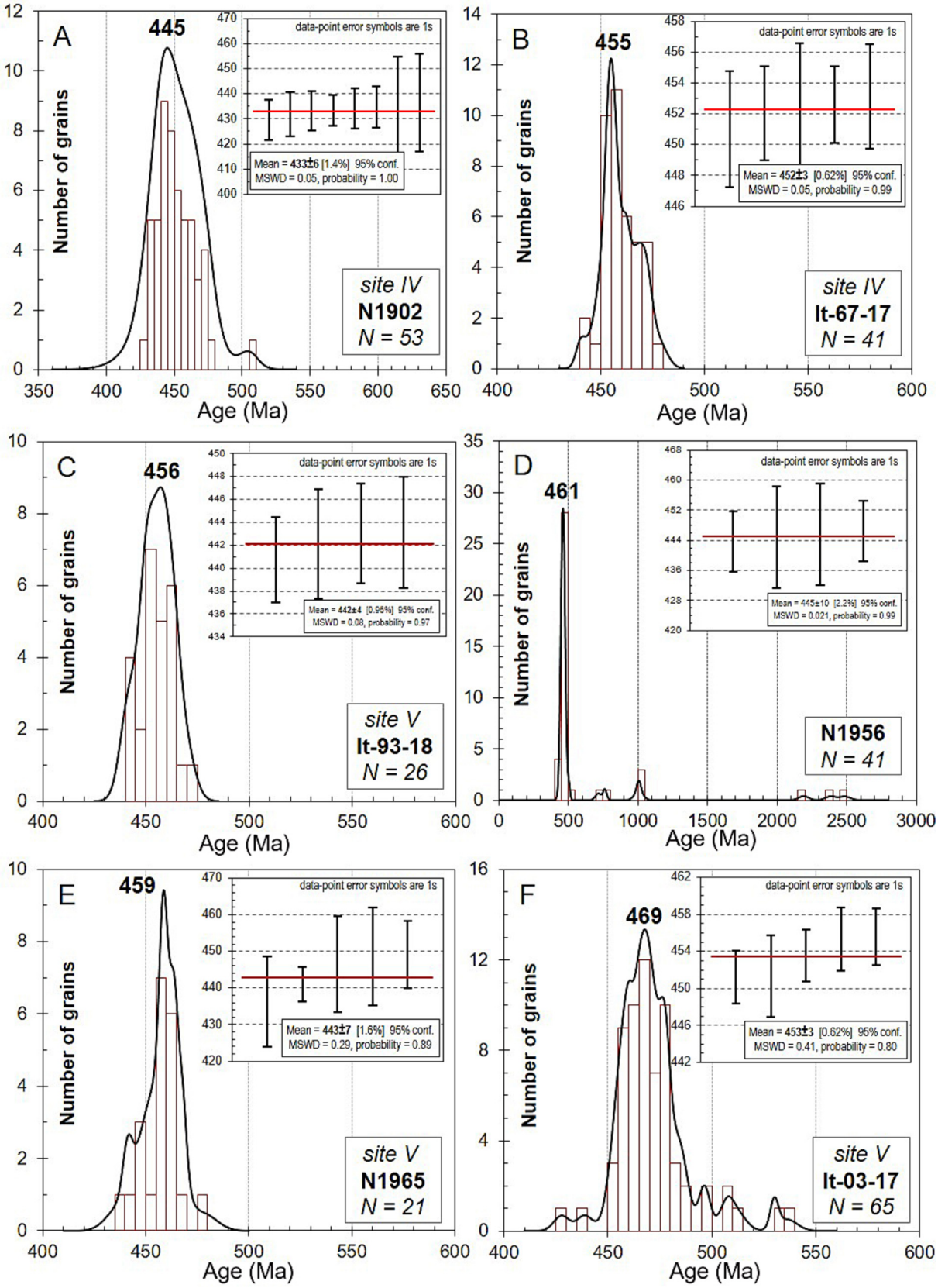

Fig. 7. U–Pb detrital zircon age data on the central part of the Itmurundy Zone (modified from Safonova et al., 2022).

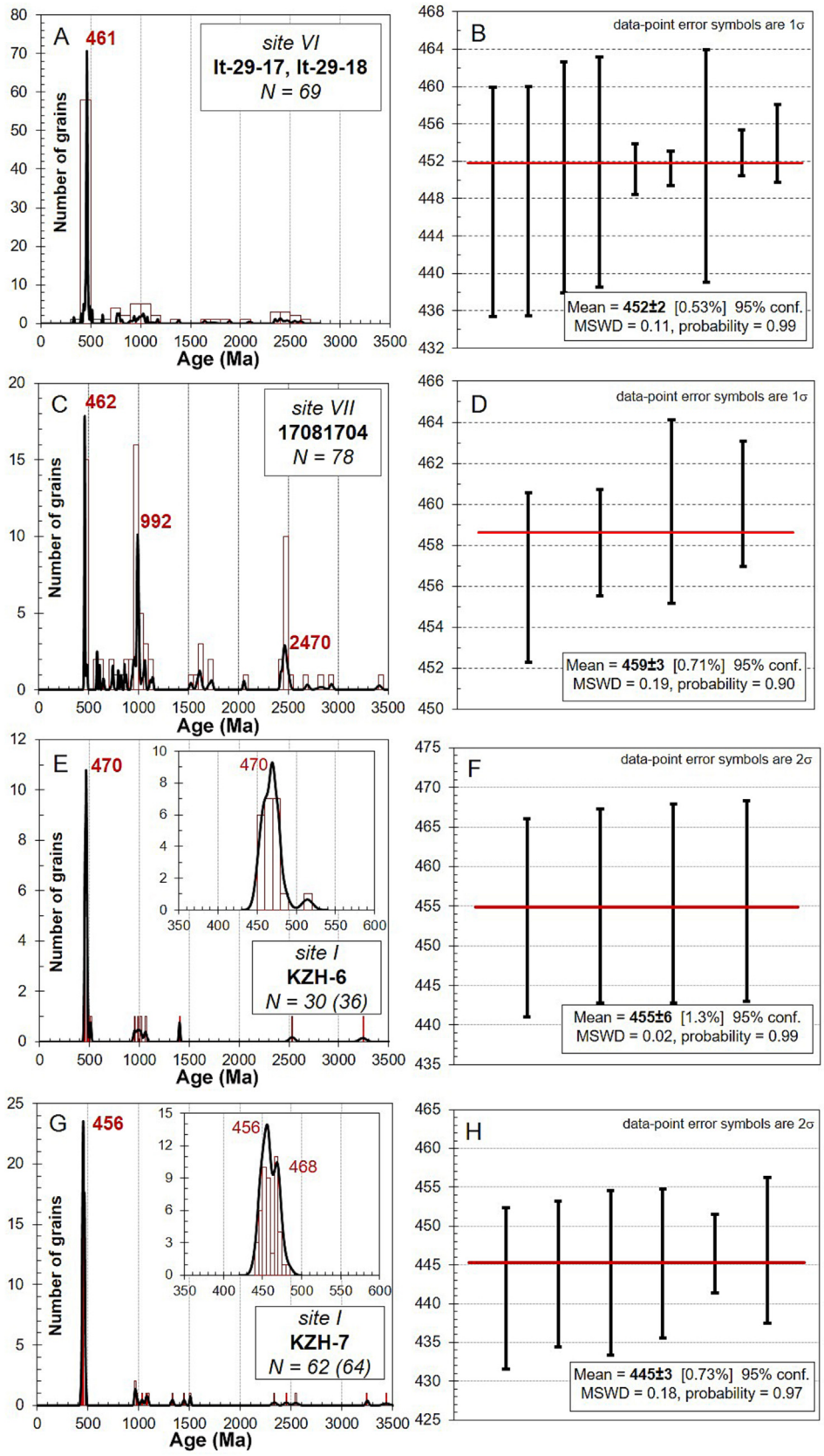

Fig. 8. U–Pb detrital zircon age data. A–D, from the eastern part of the Itmurundy Zone (Sites VI, VII, modified from Safonova et al., 2022); E–H, from the western part of the Itmurundy Zone (new data; Site I).

(Fig. 7A–F). The weighted averages of the youngest populations are, respectively, 453 ± 3 Ma (Middle Ordovician), 452 ± 3 Ma (Middle Ordovician), 443 ± 7 Ma (Ordovician-Silurian boundary), 442 ± 4 Ma (Ordovician-Silurian boundary), 452 ± 3 Ma (Late Ordovician), and 433 ± 6 Ma (Llandovery-Wenlock boundary) (Fig. 7A–F) (Safonova et al., 2022). The sandstones from the eastern part (sites VI and VII in Fig. 3) display a different style of the distributions of U–Pb detrital zircon ages: they are polymodal with minor to notable amount of Precambrian zircons (Fig. 8A, C). The U–Pb age spectra show major peaks at 461 Ma and 462 Ma (middle Ordovician) and minor peaks at 992 Ma and 2470 Ma. The weighted averages of the youngest zircons are, respectively, 452 ± 2 Ma (late Ordovician) and 459 ± 3 Ma (middle-late Ordovician boundary) (Fig. 8B, D) (Safonova et al., 2022).

Here we report new zircon data from the western part of the Itmurundy Zone, the area of the Kazyk Fm. (Site I in Fig. 3). The zircons were separated from two samples of fine- and medium-grained sandstones. Sample KZH-6 yielded 36 U–Pb ages, of which 30 showed concordant values of $^{206}Pb/^{238}U$ and $^{207}Pb/^{235}U$ ratios with a concordance higher than 95% (Supplementary Data Table S1). The distribution of the U–Pb ages is unimodal with a main peak at 470 Ma, i.e. at the early-middle Ordovician boundary, plus there are several Neoproterozoic ages (Fig. 8E). The weighted average of the youngest zircons is 455 ± 6 Ma (late Ordovician) (Fig. 8F). Sample KZH-7 yielded 64 U–Pb ages, of which 62 are concordant in respect to $^{206}Pb/^{238}U$ and $^{207}Pb/^{235}U$ ratios at a concordance higher than 95%. The distribution of the U–Pb ages is bimodal with two main peaks at 468 Ma and 456 Ma (late Ordovician) (Fig. 8G). The age population also includes several Silurian (N = 5), Neoproterozoic (N = 16) and sporadic single Archean (N = 6) zircons. The weighted average of the youngest zircons is 445 ± 3 Ma, i.e., the Ordovician-Silurian boundary (Fig. 8H).

4. OPS lithologies of the Itmurundy Zone

The micropaleontological data (conodonts, graptolites) and U–Pb zircon ages clearly indicate that the age of the OPS units of the Itmurundy Zone range from the middle Ordovician (late Dapingian) to the early Silurian (Llandovery). The ages of the supra-subduction granitoids are older showing two groups: early Cambrian and late Cambrian. Note that all those rocks occur as blocks in the serpentinite mélange, i.e. probably represent pieces of former magmatic arcs that were destroyed by subduction erosion (Safonova and Perfilova, 2023). Therefore, we do not consider them as parts of OPS. Following the OPS succession (Isozaki et al., 1990; Wakita and Metcalfe, 2005), we below review the main petrographic, geochemical and isotope, if available, data from three main groups of lithologies: oceanic floor basalts, pelagic and hemipelagic deep-water sediments and trench facies.

4.1. OPS oceanic basalts

The lower part of the OPS succession includes oceanic floor basalts formed at mid-oceanic ridges (MORB), oceanic islands (OIB) and oceanic plateaus (OPB). All those rocks have specific lithological, petrographic and chemical characteristics (e.g., Mullen, 1983; Meschede, 1986; Sun and McDonough, 1989; Kerr et al., 2000; Regelous et al., 2003; Pearce, 2008). The volcanic rocks often, but not always, occur in direct contact with OPS sedimentary rocks (Fig. 9A, B). They are represented mainly by tholeiitic basalt and andesibasalt and alkaline basalt (Fig. 9C, D), that have Mg# spanning 26–62, SiO_2 = 44.1–54.5 wt.%, TiO_2 = 1.4–4.3 wt.%; CaO = 3.2–11.1 wt.% and Al_2O_3 = 13.3–17.3 wt.% (Safonova et al., 2020; Supplementary Data Table S2). According to the content of TiO_2 we separated the basalts into two groups: high-Ti (TiO_2 > 2-wt.%) and mid-Ti (TiO_2 = 1.4–1.7 wt.%).

The high-Ti basalts are associated with volcaniclastic rocks showing signatures of slumping down and deep-sea sediments (shale, chert) (Fig. 9A, B). They are dominated by alkaline varieties (Fig. 9C) with relatively low Zr/Nb ($Zr/Nb_{av.}$ = 9.8) and high light rare-earth elements (LREE) ($La_{Nav.}$ = 122) (Supplementary Data Table S2). The subalkaline varieties are mostly tholeiitic basalts (Fig. 9D). Their spectra of rare-earth elements (REE) show enriched light components (LREE, La/Yb_N = 1.1–3.6), and differentiated heavy REE ($(Gd/Yb)_N$ = 1.3–3.2) (Fig. 9E). The differentiated HREE and the results of geochemical modelling in the Nb vs Nb/Yb system suggest derivation of parental melts by low-degree melting of garnet-bearing mantle sources (Safonova et al., 2020). The primitive mantle normalized multi-element spectra indicate that the high-Ti basalts are enriched in high-field strength elements (HFSE) and accordingly show peaks at Nb relative Th and La (Nb/La_{pm} = 0.9–1.3; Nb/Th_{pm} = 0.7–1.7) (Fig. 9F). The high-Ti basalts are characterized by positive to negative values of $\varepsilon_{Nd}(t)$ from + 4.9 to − 8.7 (Fig. 9H) that is indicative of their derivation from variably enriched mantle sources. In the $MnO\text{-}TiO_2\text{-}P_2O_5$ discrimination diagram (Mullen, 1983), they plot into the fields of oceanic island alkaline and tholeiitic basalts (Fig. 9G). All these geological and geochemical features suggest that the high-Ti basalts of the Itmurundy Zone erupted in an intra-plate oceanic setting, i.e., at oceanic islands and/or seamounts like those of the Emperor-Hawaii Chain of seamounts and volcanoes (e.g., Chen et al., 1991; Regelous et al., 2003).

The mid-Ti rocks occur in contacts with deep-sea cherts. They are mostly tholeiitic basalts (Fig. 9C, D) with higher Zr/Nb ($Zr/Nb_{av.}$ = 25) compared to the high-Ti varieties. They are less enriched in the LREEs ($La_{Nav.}$ = 23) and HFSE giving La/Yb_N = 0.8–1.0, Gd/Yb_N = 1.1–1.3, Nb/La_{pm} = 1.0 (Supplementary Data Table S3). They yielded LREE neutral/flat REE spectra similar to those of MORB (Fig. 9E). The multi-element spectra show Nb enriched relative Th, but not La (Nb/La_{pm} = 0.5–0.9; Nb/Th_{pm} = 1.4–1.6) and, in general, are similar to that of an average MORB (Fig. 9F). The mid-Ti volcanics are characterized by only positive values of $\varepsilon_{Nd}(t)$ ranging from + 4.7 to + 7.7 (Fig. 9H). In the $MnO\text{-}TiO_2\text{-}P_2O_5$ discrimination diagram (Mullen, 1983), most of the mid-Ti basalts plot in the field of MORB (Fig. 9G). Accordingly, we consider those mid-Ti volcanics as formed at mid-oceanic ridge(s). The different degrees of differentiation of the HREEs in the high-Ti and mid-Ti varieties indicate derivation of parental melts from garnet-bearing (garnet lherzolite) and garnet-free (spinel lherzolite) mantle sources, respectively (Safonova et al., 2020).

4.2. OPS pelagic and hemipelagic sediments

Both, the OIB-type and MORB-type volcanics are, as mentioned before, covered or occur in contact with OPS deep-sea oceanic sediments: pelagic (chert) and hemipelagic (siliceous mudstone, siltstone, shale). The deepest OPS sediments can be variable in color: from light to dark brown, dark and light red, amber, dark to light grey, violet, chocolate, etc. Their most distinguishable and outstanding feature is ribbon texture and presence of microfossils, radiolarians and conodonts. Such cherts are typical of all modern to older accretionary prisms and complexes (e.g., Yamamoto, 1987; Sano, 1988; Hori, 1992; Ando et al., 2001; Maruyama et al., 2010; Wakita, 2012; Kusky et al., 2013; Safonova et al., 2016). The sedimentation rate of pelagic cherts formed at greater depths of modern oceans is very low, 1–3 mm per 1000 years (Huneke and Henrich, 2011). Pelagic cherts typically cover oceanic floor MORB-type basalts, but also may be associated with OIBs at the deepest foothill parts of oceanic islands and seamounts (Sano and Kanmera, 1988).

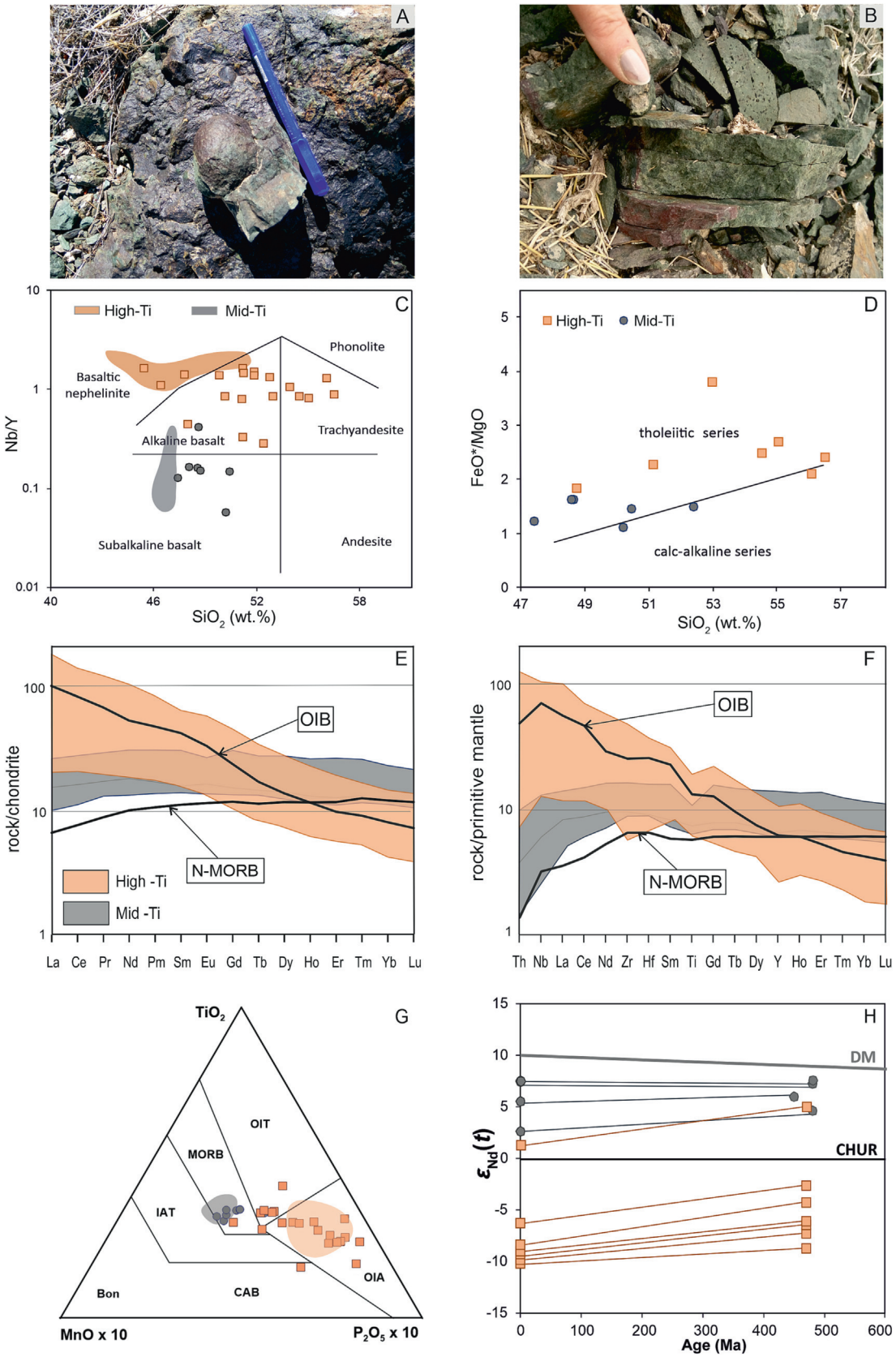

Fig. 9. Field photos and main geochemical features of oceanic floor basalts of the Itmurundy Zone. (A) Pillow basalt; (B) a contact between siliceous mudstone (violet) and basalt (green); (C) SiO_2 – Nb/Y classification diagram (Winchester and Floyd, 1977), the pink and grey fields are from (Degtyarev et al., 2020); (D) SiO_2 – FeO*/MgO plot (Miyashiro, 1974); (E, F) chondrite-normalized rare-earth element patterns (E) and primitive mantle-normalized multi-component trace element diagrams (F); (G) MnO*10 – TiO_2 – P_2O_5*10 discrimination diagram (Mullen, 1983); (H) $\varepsilon_{Nd}(t)$ versus age diagram. The normalizing values for chondrite and the data for OIB and MORB are taken from Sun and McDonough (1989). (For interpretation of the references to color in this figure legend, the reader is referred to the web version of this article.)

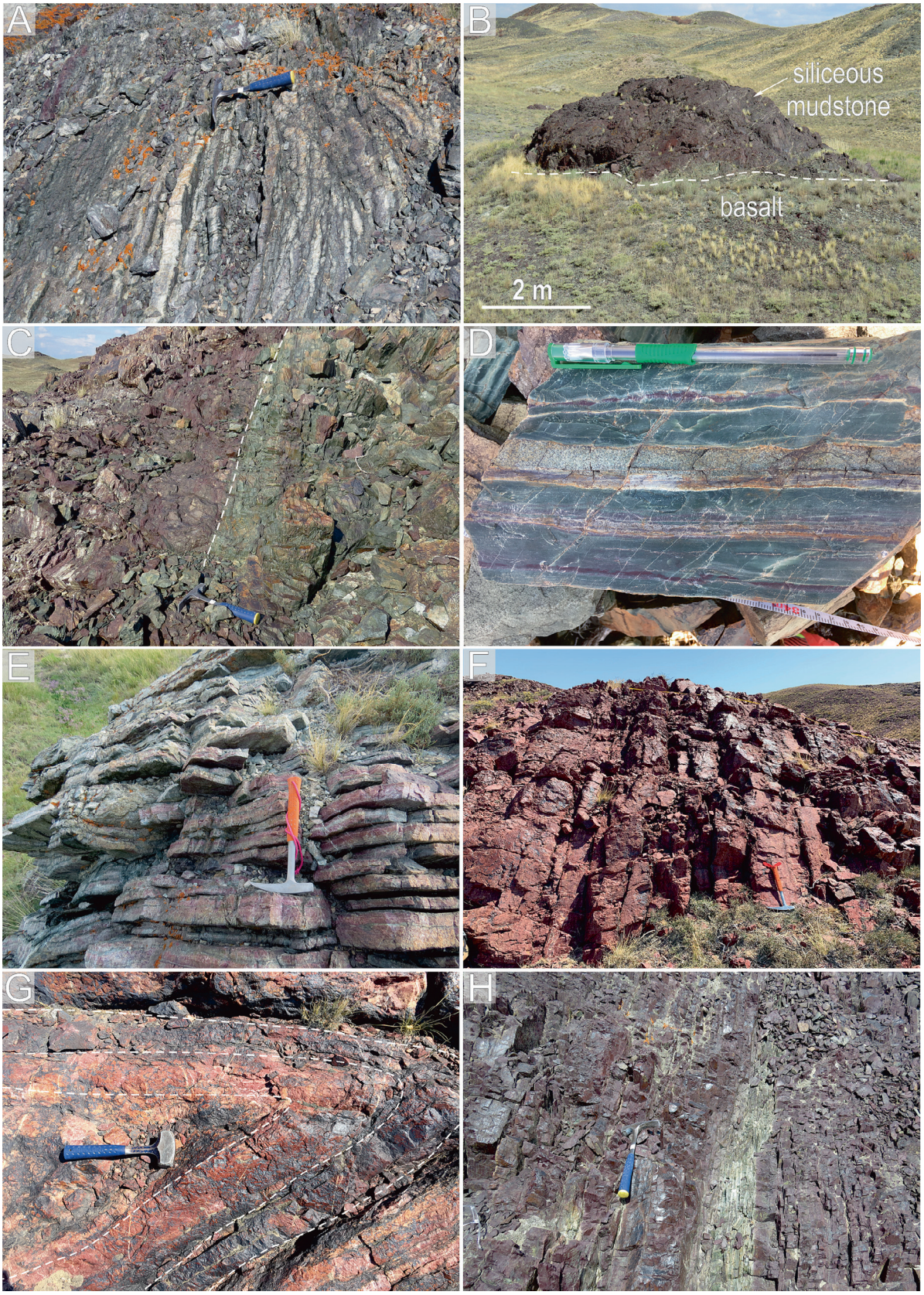

Fig. 10. Field photos of pelagic and hemipelagic oceanic sediments of the Itmurundy Fm. (A–D) and Kazyk Fm. (E–H). (A) Ribbon chert; (B) a contact between chocolate siliceous mudstone and basalt; (C) green and chocolate siliceous mudstones; (D) bedded black shale; (E, F) pelagic cherts; (G) a fold in chert; (H) siliceous mudstone with ribbon texture. (For interpretation of the references to color in this figure legend, the reader is referred to the web version of this article.)

In the Itmurundy Zone, the cherts have been found at outcrops of all formations, but are more abundant in the Kazyk Fm. (Figs. 5 and 6). The cherts of the Itmurundy Fm. are massive to ribbon textured (Fig. 10A), grey, brown to dark brown (chocolate) and in places occur in contact with basalt (Fig. 10B). The siliceous shales are violet, greenish and black, also may lie directly upon basalts of OIB-type (Fig. 10C, D). The cherts of the Kazyk Fm. are dominantly ribbon and red, amber and brown–red in colors (Fig. 10E-G). The Kazyk chocolate mudstones may also have ribbon textures (Fig. 10H). Siltstones and shales are less abundant compared to the Itmurundy Fm. (Safonova et al., 2019).

4.3. OPS trench facies

Coarser-grained clastic rocks, gravelstones and greywacke sandstonesoccur in all formations of the Itmurundy Zone, in places, as parts of turbidite associations (Fig. 11A, B). The grey and greenish grey fine-to coarse-grained sandstones are poorly sorted and have massive textures. The angular to poorly rounded clasts aremafic to andesitic volcanic rocks, sedimentary rocks, plagioclase, and, to a lesser degree, K-feldspar and quartz. The volcanic rocks in clasts (0.1–1.0 mm) possess hyalopylitic, intercertal, microlithic and poikiloophitic structures. The sedimentary rocks in 0.1–0.8 mm clasts are chert and siliceous mudstone. The grains of plagioclase and quartz are 0.1–0.8 and 0.1–0.3 mm in size, respectively. The typical accessory minerals are zircon, tourmaline, epidote and Fe-oxides. There is no cement in the sandstones, but the matrix only, which composition is close to that of the clasts. The sandstones from sites VI and VII carry more grains of quartz (0.2–2.0 mm) and felsic rocks (granite, dacite). The classification of Shutov (Shutov, 1967), which is based on the counting of clasts of this or that type, shows that the sandstones from sites I-V are greywackes, feldspar and quartz-feldspar greywackes, while those from sites VI-VII are greywacke arkoses (Supplementary Data Fig. S3).

In general, the Itmurundy sandstones are enriched in MgO and Fe_2O_3, but show less Al_2O_3 relative the Post-Archean Australian Shale, PAAS (Supplementary Data Table S3). The concentrations of SiO_2 in the sandstones from sites I–V span 55.2 wt.% to 72.6 wt.%, while those from sites VI and VII are more felsic (SiO_2 = 52.6–74.6 wt.%). However, the ratio of SiO_2/Al_2O_3 for all sandstones is below 8.5 indicating fast burial of the sediments, i.e., close to the provenance (Pettijohn et al., 1972). The sandstones from sites I–V are more ferruginous ($Fe_2O_{3av.}$ = 6.7 wt.%) relative those from sites VI–VII ($Fe_2O_{3av.}$ = 5.9 wt.%) suggesting more mafic igneous rocks in the provenance of the former (Taylor and McLennan, 1985). According to the classification of F. Pettijohn (Pettijohn et al., 1972), the Itmurundy sandstones are greywackes and litharenites (Fig. 11C). The geochemical indexes CIA and ICV, CIA = $[Al_2O_3/(Al_2O_3 + CaO + Na_2O + K_2O)] \times 100$ (Nesbitt and Young, 1982), ICV = $(CaO + K_2O + Na_2O + Fe_2O_3 + MgO + MnO + TiO_2)/Al_2O_3$ (Cox and Lowe, 1995), indicate that the sandstones are immature and derived from low-weathered rocks once present in the provenance (Fig. 11D). The values of CIA for the sandstones from sites I–V are lower than those for the sandstones from sites VI–VII indicating a lower degree of weathering in the provenance. More evidence for a more mafic source of the sandstones from sites I–V comes from the higher concentrations of Sr and their positive correlation with Fe (Feng and Kerrich, 1990). The concentrations of REE are all lower than in the PAAS, and the multi-element spectra show troughs at Nb-Ta (Supplementary Data Table S3; Safonova et al., 2022), similar to those typical of supra-subduction igneous rocks (Pearce, 1982; Briqueu et al., 1984). The tectonic diagrams show that the sandstones from sites I–V formed by destruction of an intra-oceanic (Fig. 11E) or undissected (Fig. 11F) arc, while those from sites VI and VII were derived from a continental arc or a recycled orogen (Bhatia, 1983; Dickinson et al., 1983; Safonova et al., 2022).

5. Detailed description of OPS sites

In this section we present first results of the detailed mapping of igneous and sedimentary rocks of the three "initial" formations (section 3.2), Itmurundy, Kazyk and Tyuretai, that we made in 2017–2019 at seven sites of the Itmurundy Zone, in its western, central and eastern parts (Fig. 3). These sites including typical OPS lithologies: ocean floor basalt – pelagic chert – hemipelagic siliceous sediments – trench clastics (Fig. 1). The western part includes Site I and Site II in the vicinity to Karajal Mt. and 457 Mt., respectively. Sites III, IV and V are located in the central part, near Ushtogan Mt., East Arkharsy Massif and 422 Mt., respectively. In the eastern part, we studied sites VI «OD-1» and VII «OD-2» (see also Supplementary Data Figs. S1-S2 For location and photos).

5.1. Western Itmurundy Zone

Site I (Karazhal or Karajal; Fig. 3): thick beds of red and brown cherts are intercalated with yellowish and light-brown siliceous mudstones and siltstones and overlapped by sandstones (Fig. 12). Pillowed and sheared basalts (OIB-type; Supplementary Data Table S2) occur at the base of the mudstones, often as lenses. The visual thicknesses of the cherts are significantly larger than those of the siliceous sediments and sandstones. The age interval inferred from conodonts spans late Darriwilian to early Katian (Table 1) (Zhylkaidarov, 1998). The summarized lithological column is around 200 m thick (Fig. 13a), but we must account that the packages are probably duplexes as they are parts of the accretionary complex and most boundaries between the chert-mudstone packages are tectonic or concealed (Fig. 12A). The MDA of sample KZH-7 (445 Ma) is younger than that of KZH-6 (455 Ma) suggesting the direction of subduction to the northwest (Figs. 3, 8F, H, 12B).

Site II (Mt. 457) is located southeast of Site I (Fig. 3). There are two rocks associations: basalt-chert in the east and chert-siltstone-breccia in the west (Fig. 14A). The thick basaltic unit includes numerous lenses of deformed reddish and greenish chert and motley siliceous mudstones (Supplementary Data Fig. S2A, B). The sedimentary unit of the Kazyk Fm. consists of chert, variably colored siliceous siltstone and volcanogenic-sedimentary breccia. The geological map shows that the basaltic and sedimentary units can be attributed to the Itmurundy and Kazyk fms., respectively (Fig. 3). But in terms of OPS, we can also consider these two units as parts of an oceanic seamount with the sediments formed at its slopes (siliceous siltstone, breccia) and the foothill (siliceous mudstone, chert) (e.g., Safonova, 2009; Safonova and Santosh, 2014). The age interval inferred from conodonts in chert spans middle Darriwilian to early Sandbian (Table 1) (Novikova et al., 1983).

5.2. Central Itmurundy Zone

Sites III (Ushtogan) and IV (East Arkharsu) (Fig. 3) are dominated by basalt and volcanogenic breccia and gravelstone of the Itmurundy Fm. (Fig. 13b, 14B, C). Sedimentary rocks, mostly siliciclastic and cherty, are present as well but their thicknesses are variable. The basalts often occur as pillow-lavas and flows. The pillows are from 50 cm to 1 m in diameter, in places, they are strongly sheared and carry variably oriented slickenlines (Supplementary Data Fig. S2C, H). Sporadically outcropped siliceous sediments, tuffs and turbidites occur as lenses and boudins. The siliceous sediments are strongly deformed to form overturned folds and "horse" structures or duplexes (thrusts) and recrystallized to form mullion

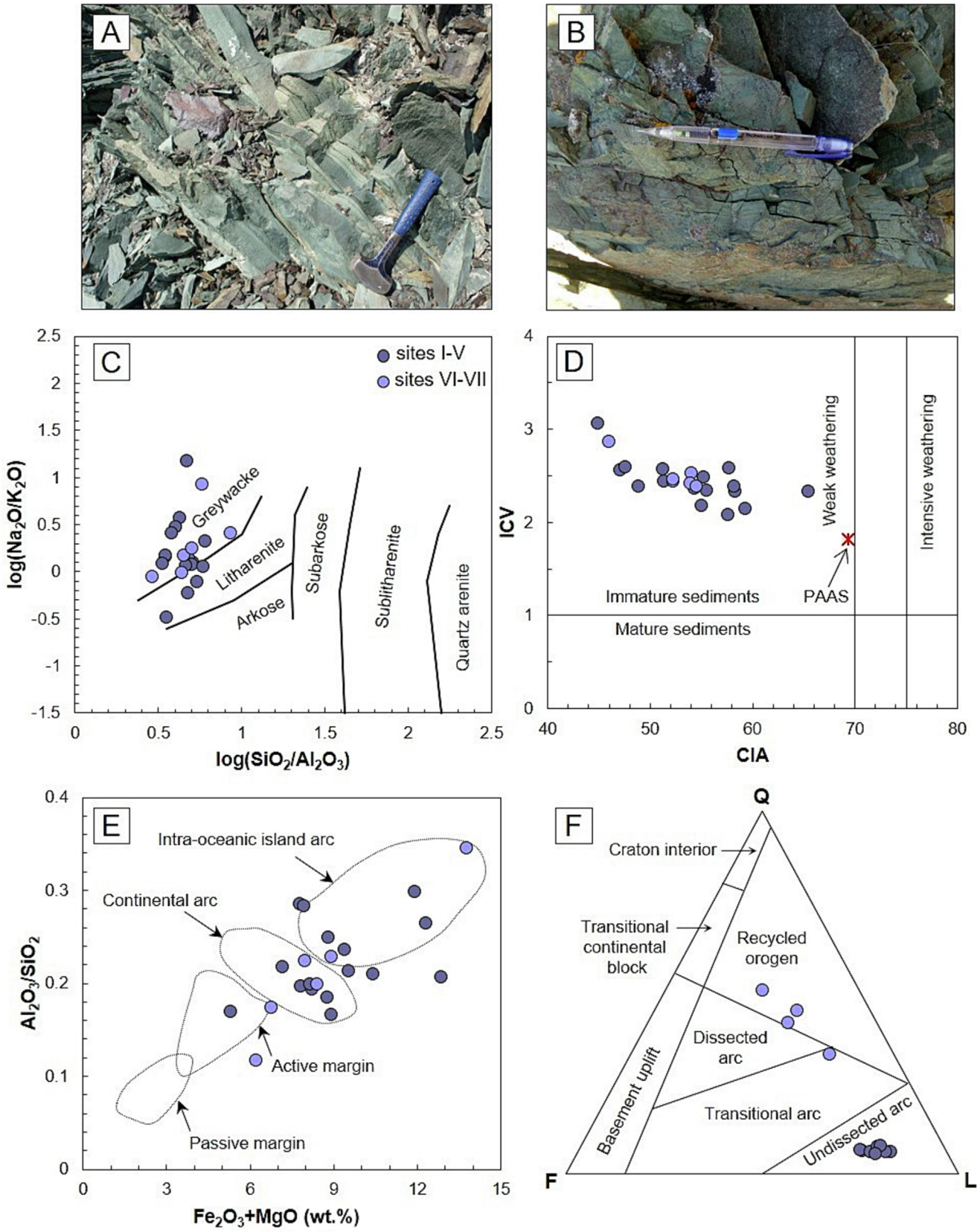

Fig. 11. Field photos and main geochemical features of greywacke sandstones of the Itmurundy Zone. (A) Turbidite of the Itmurundy Fm. (Site IV); (B) sandstones of the Tyuretai Fm. (Site VI); (C) classification diagram (Pettijohn et al., 1972); (D) CIA-ICV diagram (Nesbitt and Young, 1982; Cox and Lowe, 1995) (see section 4.3); (E) geochemistry-based discrimination diagram of (Bhatia, 1983); (F) petrography-based discrimination diagram of Dickinson et al. (1983). The value for PAAS is after Taylor and McLennan (1985).

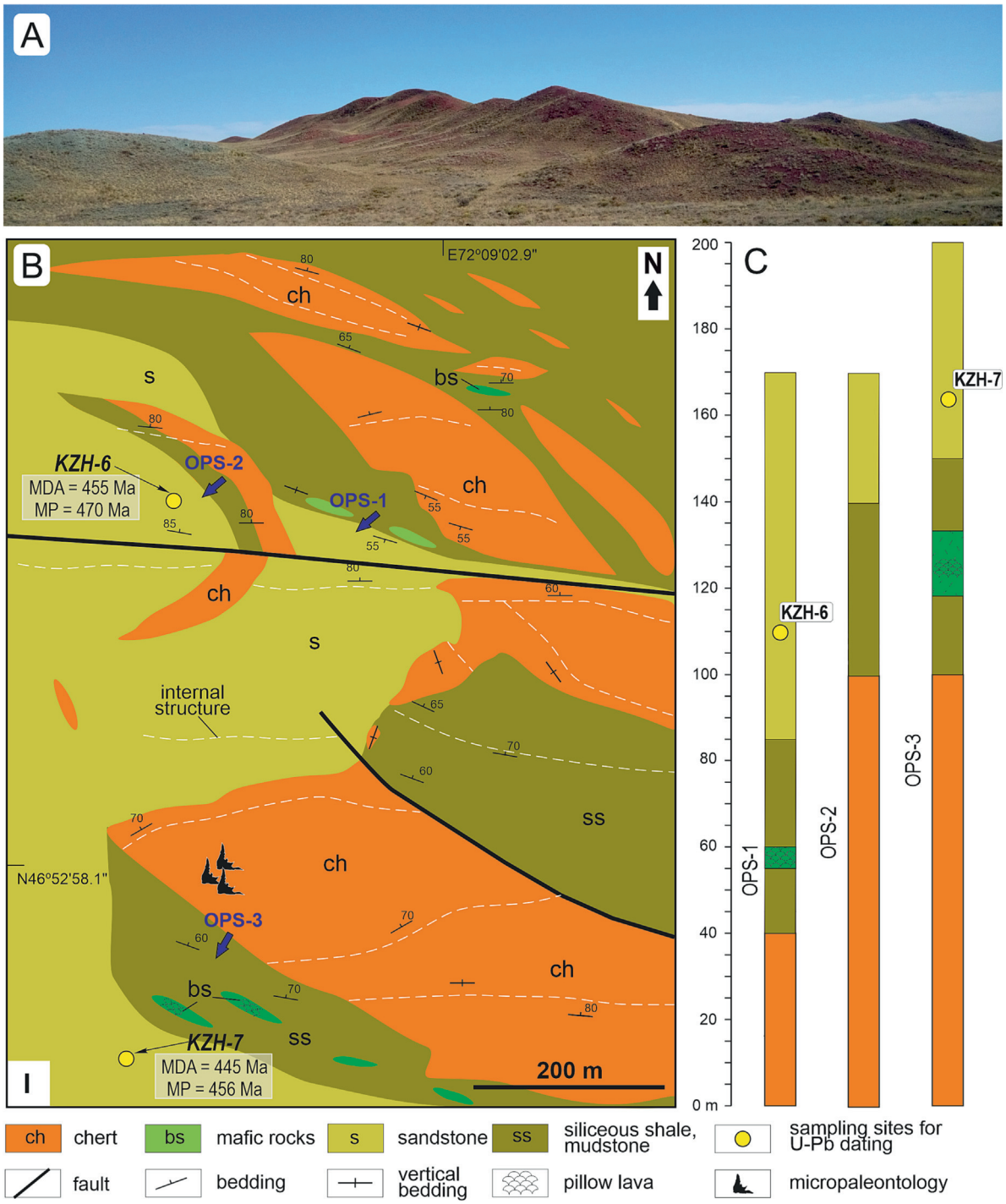

Fig. 12. Site I, Kazyk Fm. (A) A general photo of parallel-bedded chert-mudstone packages; (B) detailed geological scheme; (C) lithological columns (for location see B).

structures (Supplementary Data Fig. S2D). The turbidites are composed of medium-grained sandstones interbedded with siliceous mudstones (Fig. 11A). The breccias consist of angular fragments of chert, siliceous mudstones and siltstones, sandstones, and basalts in silty-sandy matrix (Supplementary Data Fig. S2F–G). The summarized lithological column made for Site IV is around 250 m thick (Fig. 13b). The age interval inferred from conodonts in cherts is late Darriwilian – early Katian (Nikitin, 2002; Degtyarev et al., 2020), but another chert sampled in Site IV yielded a larger interval of middle to late Darriwilian (Table 1) (Degtyarev et al., 2020). The MDA of the sandstones from Site IV is younging from 452 Ma to 433 Ma to the southeast suggesting the subduction to the northwest (Fig. 7A, B, 14C). More evidence for that direction of subduction comes from the microfossil age constraints from in Site III, that also get younger from NW to SE, from Darriwilian to Sandbian (Fig. 3).

Site V (Mt. 422). There are outcrops of various OPS sedimentary lithologies, basaltic and siliciclastic, and ultramafic rocks (Figs. 13c–e and 14D). The flows of basalt, probably Itmurundy Fm., carry lenses of chert (Supplementary Data Fig. S2H). The siliceous-clastic unit consists of intercalated chert, siliceous mudstone, siltstone, polymictic sandstone and gravelstone and proba-

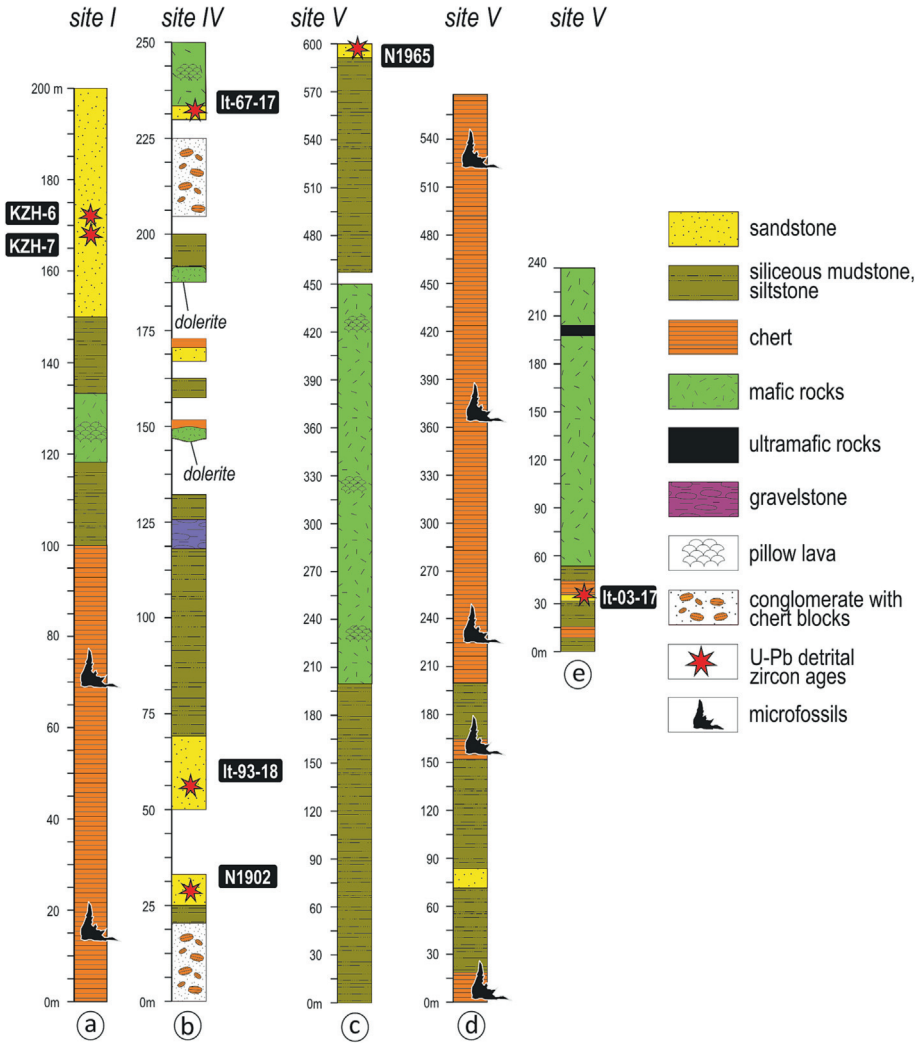

Fig. 13. Lithological columnar sections: a, for Site I, b–e, for Sites IV-V (Fig. 3) showing thicknesses, main lithologies and places of sampling of chert and siliceous mudstone for microfossils and sandstones for zircons. For details on microfossils see Table 1 and for those on zircon ages see Supplementary Data Table S1 and Figs. 7 and 8.

bly belongs to the Kazyk Fm. (Fig. 13c–e). The Kazyk sediments may appeared thrust over the Itmurundy Fm. (Fig. 14D). The cherts form overturned folds with steeply dipping flanks and westward striking hinges, flexural or monocline, and scalloped folds (Supplementary Data Fig. S2I). The hemipelagic sediments are represented by thick green and dark-red siliceous mudstones and siltstones hosting interbeds of sandstones and cherts and lenses of basalt. In addition, there are outcrops of boudinated dunite and serpentinite with veinlets of chlorite and asbestos. The visual thickness of the OPS packages can reach 600 m, but, again, most contacts are tectonic and therefore the duplexing could be a case. The age interval inferred from conodonts in cherts is also late Darriwilian – early Katian (Safonova et al., 2019). The MDA of the sandstones from Site V is also younging from 453 Ma to 443 Ma, i.e. to the southeast (Fig. 7C, E, F, 14D).

5.3. Eastern Itmurundy Zone

Sites VI (OD-1) and VII (OD-2) are located in the eastern part of the Itmurundy Zone and compose large anticline structures, which axial planes are striking from NW to SE (Fig. 3). The outcrops are rare (Fig. 15) (Safonova et al., 2022) making their detailed mapping, in particular, in terms of columnar sectioning, impossible. The cores of the folds consist of basalt and thick sandstone (samples It-29–17 and It-29–18 in Fig. 15, Site VI) and their flanks are composed of chert, siliceous mudstone, siltstone and grey sandstone with large lenses of volcanic rocks. There are also zones of breccias, which fragments are basalt, chert, siliceous mudstone and siltstone. The cherts are strongly fractured and recrystallized. The microfossil ages constrains are the period from the late Darriwilian to the early Katian (Table 1) (Nikitin, 2002; Degtyarev et al., 2020). The zircon-based MDA of the sandstones sampled in Site IV (452 Ma) is older than that of Site VII (459 Ma) (Figs. 3, 8B, D, 15) (Safonova et al., 2022) suggesting that the subduction was in a direction different from that inferred from Sites I–V.

6. Types of OPS and modes of accretion

While approaching the subduction zone, the rocks of the oceanic plate or OPS get deformed and then accreted to the hanging wall (Fig. 1A). The OPS units get detached from the subducting plate along a surface of decollement (Fig. 1B) (e.g., Isozaki et al., 1990; Kimura and Mukai, 1991; Kuramoto et al., 2000; Kusky et al., 2013; Wakita, 2015; Safonova et al., 2016). Sandstones and hemipelagic facies get detached first, then go pelagic sediments and, finally, volcanic rocks of oceanic rises (OIB), oceanic floor (MORB) and deeper ophiolites (gabbro, ultramafics). The incorporation of rocks of different origins (sediments, volcanics, etc.) into

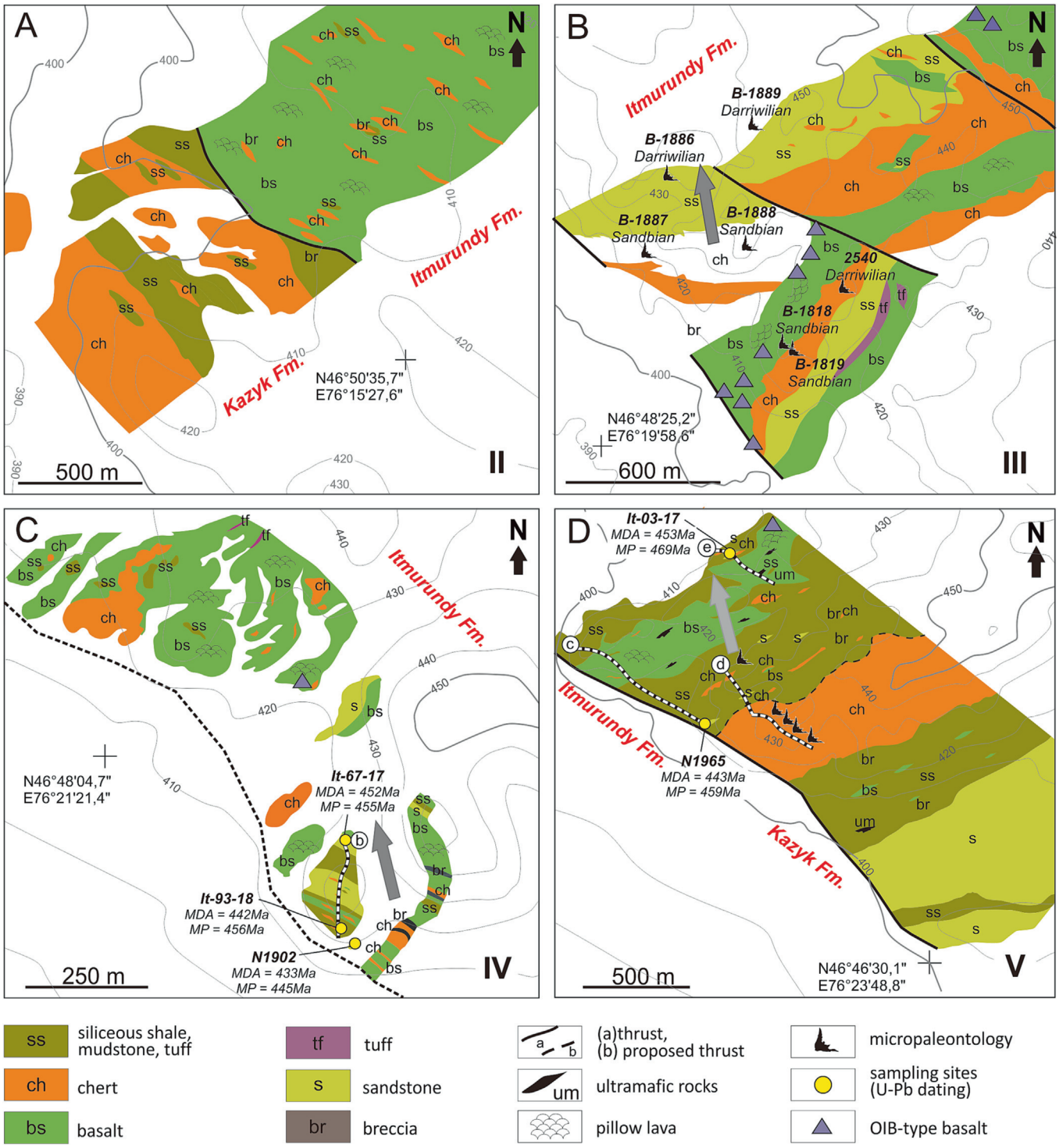

Fig. 14. Detailed geological schemes for sites II–V (for location see Fig. 3). Profiles B–D (dashed) match the respective columnar sections in Fig. 13. The grey arrows indicate a proposed subduction polarity based on microfossils age constraints (B) and U–Pb detrital zircon ages (C, D).

accretionary prism along a convergent plate boundary forms OPS horses thrust over and under each other (e.g., Wakita, 2012, 2015; Kusky et al., 2013; Wakabayashi, 2015; Ackerman et al., 2019). So, any accretionary prism consists of regularly repeated OPS horses (Fig. 1), however in old Pacific-type orogenic belts the accreted OPS units often look chaotic and accordingly often called not a prism, but a complex. Separate horses, chert-shale or chert-shale-sandstone or basalt-chert-shale packages, are thrust under each other to form duplexed structures. The tectonic/thrust boundaries between the horses are often blurred as the accreted sediments are still water-saturated and, therefore, elastic. In such cases, it is hard, if not impossible, to understand, where is a stratigraphic top/bottom and, therefore, the traditional way of stratigraphic subdivision based on Steno's law is not applicable. Each

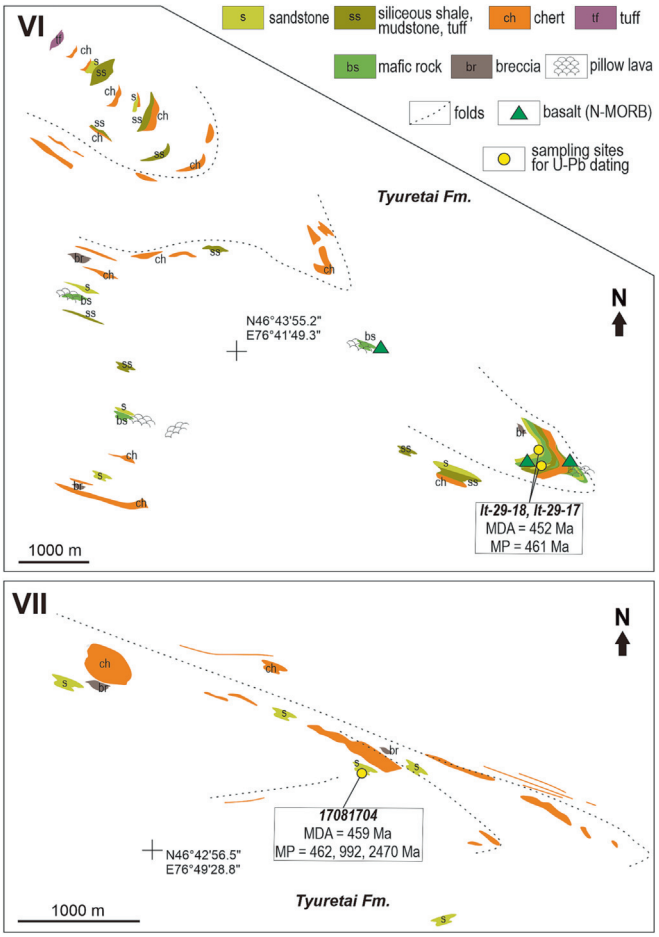

Fig. 15. Detailed geological schemes for sites VI-VII (for location see Fig. 3).

horse may appear both at the top or bottom. However, the succession from basalt to chert, then hemipelagic sediment and, finally, sandstone, remains persistent within each horse.

The results of our detailed mapping show that the basalt-chert, chert-mudstone-siltstone and siltstone-sandstone packages of the Itmurundy Zone are not chaotic, but regularly interbedded and have similar vergence (Figs. 3 and 14). The contacts between separate packages are often concealed, suggesting their tectonic character. The lithological columnar sections (Figs. 12–14) are similar to those observed in younger accretionary prisms of the western Pacific (Wakita and Metcalfe, 2005; Wakita, 2012). This confirmed the accretionary nature of the whole zone. The highlighted rock assemblages match the three "initial" formations, Itmurundy (basalt-dominated), Kazyk (chert-dominated) and Tyuretai (clastic) (Figs. 12 and 13) (Patalakha and Belyi, 1981). Our mapped Itmurundy lithologies and their in-field relationships fit the OPS succession and typical accretionary prism structures: (1) mafic volcanics, basalt and andesibasalt, typically occur at the base of the sections or packages; (2) the packages of siliceous sedimentary rocks and basalts are separated by faults; (3) the bedding of chert, siliceous hemipelagic sediments and sandstones is very steep to vertical; (4) numerous horse-structures or duplex structures with clear bottom thrusts; (5) abundant gravelstones and breccias often associated with lithologies typical of oceanic seamounts, OIB, slope facies (Figs. 12–14; Supplementary Data files).

In seven sites (Fig. 3) we distinguished three typical OPS successions: (1) pelagic ribbon cherts – hemipelagic siliciclastics – sandstones; (2) ultramafic rocks – basalts – cherts – hemipelagic siliciclastics – sandstones; (3) basalt-hemipelagic siliciclastics – sandstones (Fig. 16). Type 1 is special for thick beds of chert, while Types 2 and 3 are special for the presence of OIB-type and MORB-type basalts, respectively. Accordingly, we name these OPS successions: Chert-dominated (Type 1), OIB-hosting (Type 2), and MORB-hosting (Type 3).

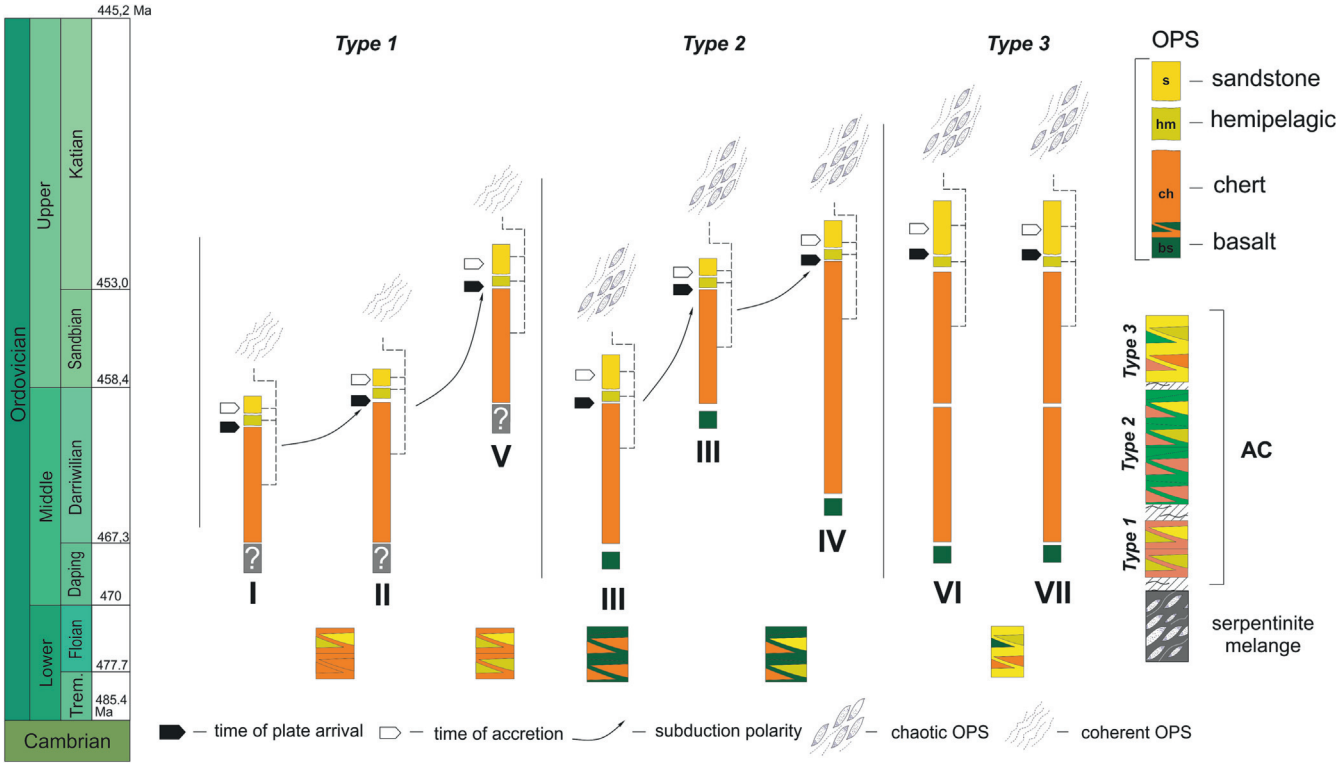

Fig. 16. Generalized lithological columnar sections showing three types of OPS of the Itmurundy AC and different styles of their accretion. I-VII, sites (for location see Fig. 3); I, Karajal, II. Mt. 457; III, Ushtogan; IV, East Arkharsu; V, Mt. 422; VI, OD-1; VII, OD-2. The age constraints are based on microfossils data (see Table 1 and references therein).

Type 1 OPS, Chert-dominated (Fig. 16), is typical of the Kazyk Fm. and has been distinguished at Site I (Mt. Karajal), Site II (Mt. 457) and Site V (Mt. 422, southern part) (Figs. 3, 12, 13a, 14A). The dominating lithologies are pelagic ribbon cherts (150–200 m thick) with much thinner interbeds of hemipelagic siliceous mudstones and siltstones (Fig. 10E–H, 12A). Sandstones are less abundant. The strata form repeated horses, but no signs of tectonic mixing. The alternation of pelagic and hemipelagic sediments indicates an oceanic plate approaching the trench. In this area, the sediments are still not consolidated and may form duplexes. The basement of Type 1 OPS could be MORB-type basalts, but not found yet. Those sediments were probably peeled directly off the oceanic floor, with minor pieces of seamount top basalts, or off a graben formed by slab bending faults (Fig. 1B, 17).

Type 2 OPS, OIB-hosting (Fig. 16), is typical of the Itmurundy Fm. and has been distinguished at Site III (Mt. Ushtogan), Site IV (East Arkharsu) and Site V (Mt. 422, northern part) (Figs. 3, 13c-e, 14B-D). Type 2 OPS is characterized by abundant basalts with lenses of ribbon chert and various thin-bedded siliceous mudstones with subordinate tuffs, turbidites and breccia (Fig. 10A–D, 11A). The small outcrops are several meters long. A special feature is a mélange of OPS rocks. That OPS mélange consists of abundant fragments of OIBs as well as siliciclastic rocks, from mudstone to sandstone. The sedimentary rocks are typically strongly deformed, brecciated. Those deformations can be caused by the slumping down of seamount sediments and by the repeated mixing of earlier and later accreted rocks like that fixed at the Akiyoshi, Mino and Shimanto accretionary complexes of Japan (Sano and Kanmera, 1988; Wakita, 2012, 2015). Large blocks of OPS sedimentary rocks keep the initial bedding and, in places, the full succession from chert to siliceous mudstone and siltstone. The arrival of a seamount to the trench can disturb the formerly accreted coherent OPS sediments and provoke turbidite currents to form chaotic structures (accretionary mélange) and turbidites, which again were involved into accretion. Evidence for that in Type 2 OPS comes from the presence of large blocks of OIB in the mélange (Fig. 16). The matrix consists of fine clastic material derived from previously accreted OPS and an adjacent arc. The U–Pb age spectra (unimodal) and the compositions (mafic to andesitic, positive $\varepsilon_{Nd}(t)$ and $\varepsilon_{Hf}(t)$) of greywacke sandstones suggest their derivation from an intra-oceanic arc (Safonova et al., 2022). The coherent cherty units, seamounts, and mélange get juxtaposed with the arc during accretion and ocean suturing (Fig. 17).

Type 3 OPS, clastic-MORB-hosting (Fig. 16), is typical of the Tyuretai Fm. and has been distinguished at Site VI (OD-1) and Site VII (OD-2) (Figs. 3, 15 and 16). Type 3 OPS is dominated by sandstones and siliceous shales (Fig. 11B) and therefore represents the upper units of OPS (Fig. 1). The lenses of MORB-type basalts (Safonova et al., 2020) and siliceous sedimentary rocks occur at the flanks of two large folds or overturned duplexes (Figs. 3 and 18) and are often submerged into a silty matrix (Fig. 15). The U–Pb age spectra (polymodal, Precambrian zircons) and the compositions (more felsic, negative $\varepsilon_{Nd}(t)$ and $\varepsilon_{Hf}(t)$) of Type 3 greywacke sandstones are different from those of Types 1 and 2 suggesting their derivation rather from a continental arc, than from an intra-oceanic arc (Safonova et al., 2022). As mostly hemipelagic and trench sediments are involved into the accretion, we may suggest that the accretion of Type 3 OPS followed a way similar to that of

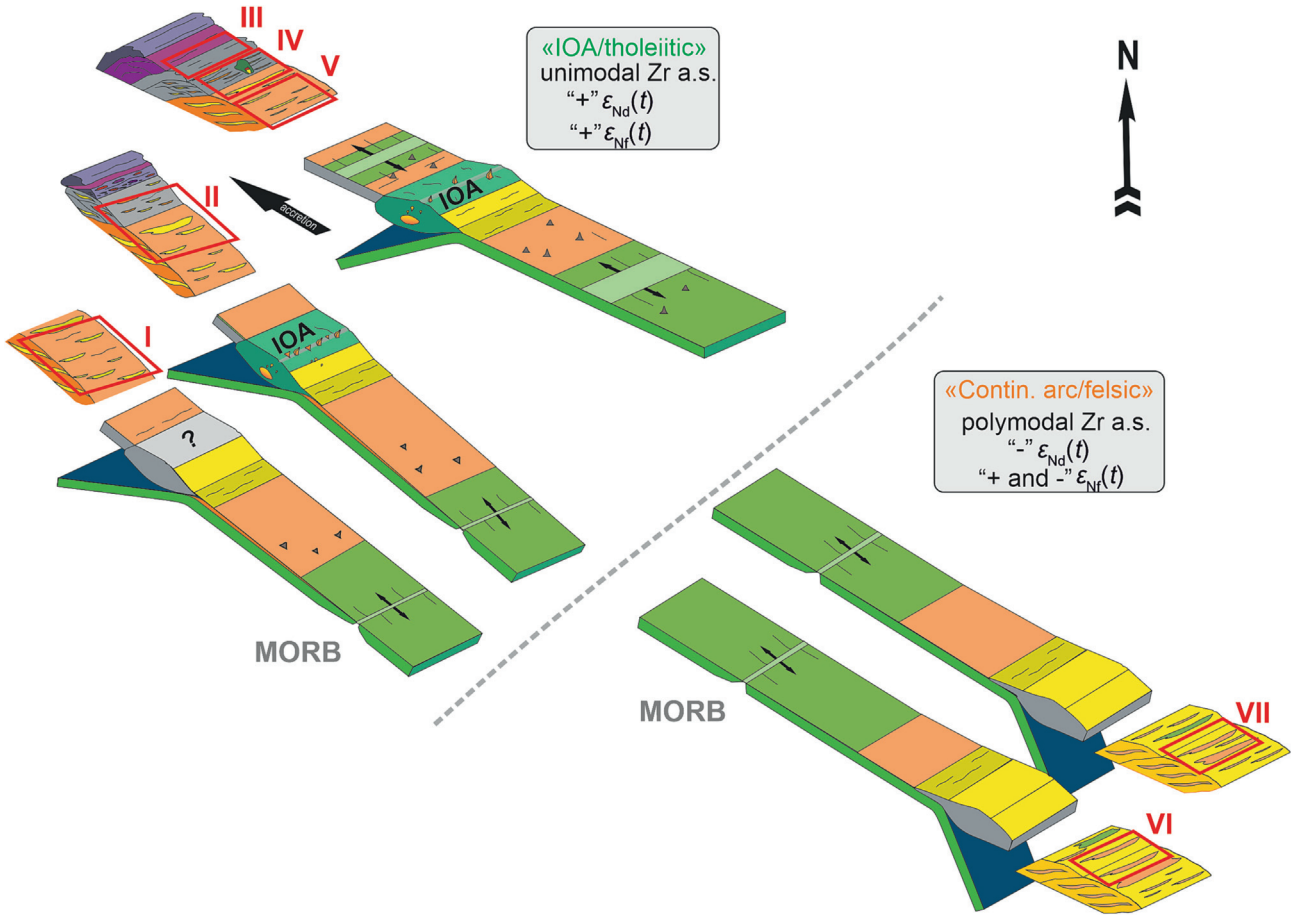

Fig. 17. Different mechanisms of accretion, arrival times and subduction polarities for OPS types 1–3. IOA, intra-oceanic arc; a.s., age spectra.

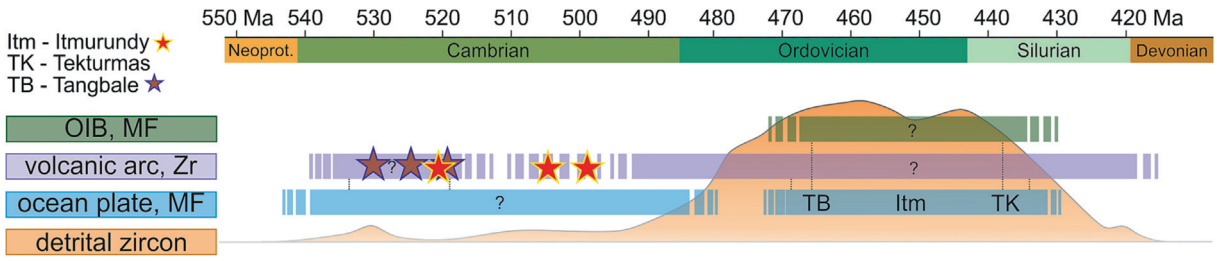

Fig. 18. The time constraints for the oceanic plate stratigraphy, periods of accretion and supra-subduction magmatism inferred from the Itmurundy Zone in comparison with the adjacent and almost coeval Tekturmas Zone to the north (central Kazakhstan) and Tangbale AC (NW China) to the south-east. Data sources: Choulet et al., 2012; Xu et al., 2013; Zhu et al., 2015; Degtyarev et al., 2017, 2020, 2021a,b; Zhang et al., 2018; Safonova et al., 2019, 2020, 2022; Zheng et al., 2019; Liao et al., 2021; Perfilova et al., 2022. Age data: MF, microfossils; Zr, zircon; Neoprot., Neoproterozoic.

Type 1 OPS. However, the mélange is present as well, that is not typical of Type 1 (Fig. 16). The Type 3 OPS sediments, pelagic, hemipelagic and trench, have been found in many accretionary complexes, for example, in the Ulaanbaatar AC of northern Mongolia (Savinskiy et al., 2021) also indicating the detachment of upper OPS units only. The presence of MORB-type basalts is not typical of accretionary complexes, as they typically get fully subducted (e.g., Safonova and Santosh, 2014; Safonova et al., 2015). The presence of MORB-type basalts as lenses in the sedimentary matrix (Fig. 15, Site VI) can be related to the mud diapirism in the lower part of a deep-sea trench caused by the pressure increasing inside the accretionary prism, like that near the Izu-Bonin-Mariana arc system (Westbrook and Smith, 1983; Johnson and Fryer, 1990; Fujioka et al., 1995; Fryer, 2012). As a result, the accretionary prism hosting Type 3 OPS incorporated the upper clastic units of OPS, i.e., sandstones and siliceous siltstones, on one hand, and MORB-type basalts of the lowermost OPS (Fig. 17).

7. OPS and the timing of accretion

The OPS siliceous-clastic sedimentary rocks are of special importance to local mapping and regional tectonics as they provide relative timing and absolute time constraints on the periods of subduction and accretion (e.g., Isozaki et al., 1990; Wakita, 2015). The relative timing means earlier or later arrival of OPS to the subduction zone and subsequent accretion (Fig. 17). The time constraints are the microfossils ages of pelagic and hemipelagic sediments and the U–Pb ages of detrital zircons from trench sandstones. The microfossils data allow reconstructing (1) an initial stratigraphic succession, i.e. OPS (Figs. 12 and 13) (Matsuda and Isozaki, 1991; Hori, 1992; Wakita, 2012), (2) the minimal parameters of an oceanic plate by the lower to upper ages of oceanic sediments, both pelagic and hemipelagic, and (3) their arrival to the trench by the upper ages of hemipelagic sediments (Table 1; Figs. 5, 6 and 13). The U–Pb ages of detrital zircons fix the beginning of accretion (the lower detrital zircon ages within the main peak) and its cessation, i.e., MDA (Figs. 7 and 8).

The tectonic history of the Itmurundy AC spans a period of about 100 Ma (Fig. 18) and its formation is linked to the subduction of oceanic plates under intra-oceanic arc(s) and/or continental arc (s) (Degtyarev, 1999; Safonova et al., 2020, 2022; Degtyarev et al., 2021a). The lower age boundary of the oceanic plate, which OPS units are present at Itmurundy sites I-V, is early Darriwilian (Fig. 6) or even Dapingian (Table 1; Nikitin, 2002), i.e., at about 467 Ma. The minimal 200 m thickness of the siliceous sediment (Fig. 14) suggests great depths and an oceanic plate comparable in size with the Indian Ocean. The low rates of sedimentation of the Itmurundy cherts (sections 3.2, 4.2) indicate a setting similar to that of the accumulation of Mesozoic to Cenozoic deep-sea cherts.

The Ordovician accretion in the western PAO formed three types of OPS in the Itmurundy AC (Fig. 16). The periods of accretion of about 40–45 Myr, 50–55 Myr and 2–8 Myr and the arrival times at ca. 490 Ma, 475 Ma and 460 Ma have been estimated for these three types, respectively (Figs. 7, 8, 17 and 18). The OPS Type 1 sandstones (western zone, Site I) were probably derived through destruction of a long-lived Ordovician arc, 480–450 Ma, and their active sedimentation started at 455 Ma (Fig. 8E–H). The OPS Type 2 hosted sandstones (central zone, Sites III-V) derived from a Late Ordovician arc (460–450 Ma) and their accumulation started in the late Ordovician and continued until the early Silurian (Fig. 7). The Type 2 sandstones could be accumulated in a basin different from Type 1 sandstones as they carry no Precambrian zircons (Figs. 7, 8E–H). The OPS Type 3 sandstones are different from those of Types 1 and 2 both lithologically and chemically (Fig. 11) and could be formed by destruction of late Ordovician igneous rocks of different origin (continental arc), composition and mantle sources (Safonova et al., 2022). Note, the sandstones of all types carry negligible to nil amounts of late Cambrian zircons, but there are Cambrian supra-subduction plagiogranites and diorites present as blocks in serpentinite mélange (Fig. 3) (Safonova et al., 2020; Degtyarev et al., 2021a). However, there is a lot of Precambrian zircons in the Type 3 sandstones suggesting older rocks in the provenance. Thus, based on U–Pb ages, geochemical, whole-rock Nd and Hf-in-zircon data, and the absence of continental material in sandstones of sites I–V (Fig. 11) (Safonova et al., 2022), two tectonic settings have been reconstructed in the Itmurundy Zone: oceanic plate – intra-oceanic arc – back-arc basin – continent, OPS Types 1 and 2, and oceanic plate – continental arc/continent, OPS Type 3 (Fig. 17). Conclusively, the three types of OPS are characterized by different times of their arrival (490 Ma, 475 Ma and 460 Ma) to the subduction zone and different periods of accretion (40–45 Myr, 50–55 Myr and 2–8 Myr). In general, the accretion started in middle Ordovician time and continued until the Wenlock (early-mid Silurian) (Fig. 18).

8. Subduction polarity

A robust reconstruction of subduction polarity or direction of subduction is possible only through a careful study of accretionary complex to understand which part of OPS arrived early and which later (Fig. 1B). The available time constraints from microfossils and zircons (MDA) clearly show that the directions of younging sedimentation ages in the western and central sites (I–V) are different from those in the eastern sites (VI–VII) (Fig. 3). In the western and central parts, the MDA of sandstones in Sites I, IV and V and the microfossils ages of cherts sampled at Site III (Fig. 3) are all younger in the southern packages than those in the packages located to the north or north-west. The ages are, respectively, 445 Ma and 455 Ma for Site I, (Fig. 12), Sandbian and Darriwilian

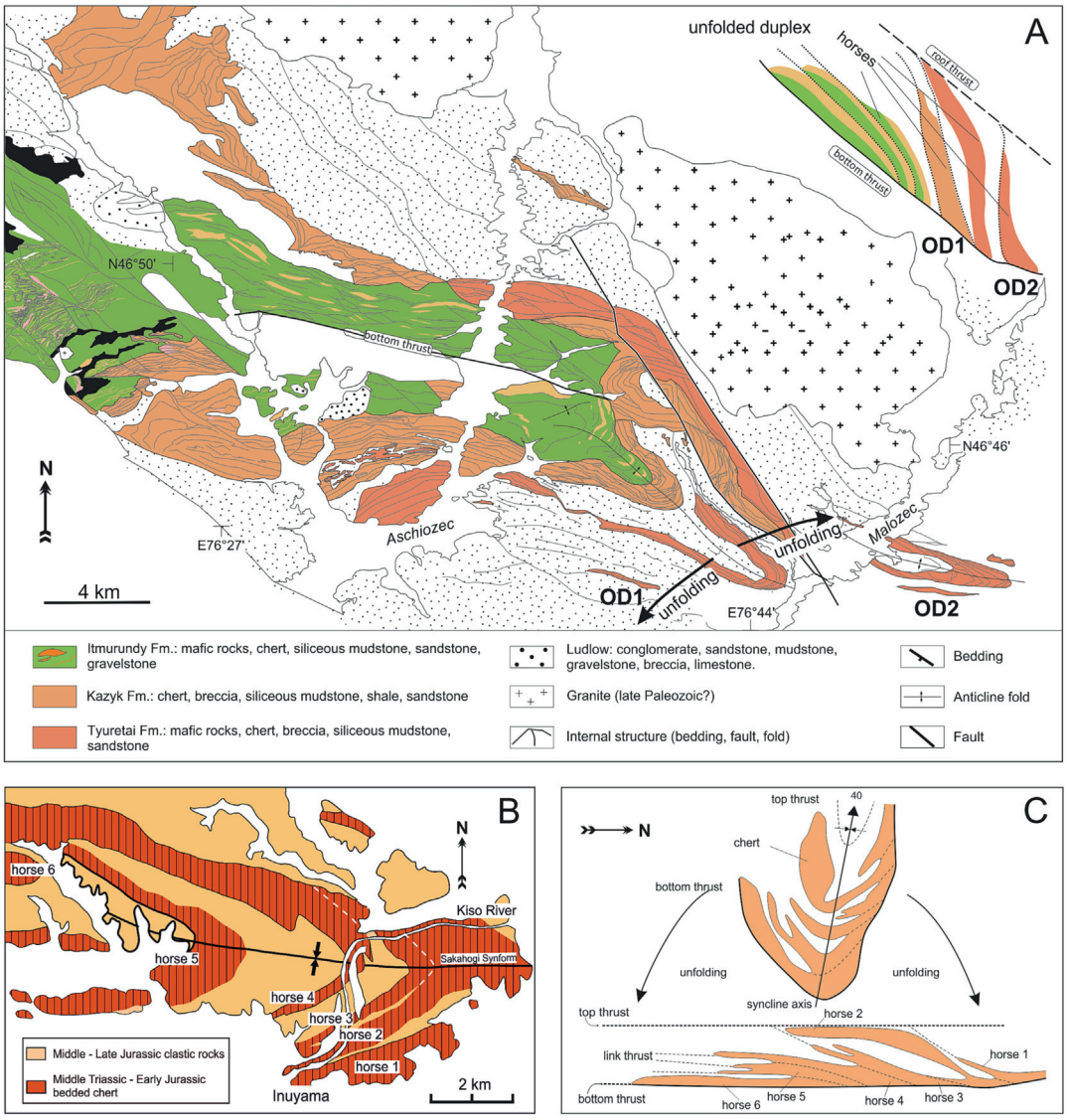

Fig. 19. Duplexes in accretionary complexes, overturned and unfolded. (A) A scheme of the Itmurundy Zone (eastern) (location see in Fig. 2) with overturned/folded duplex structures OD-1 and OD-2 (a probable "initial" position, before the overturn, of OD-1 and OD-2 OPS units is shown in the right upper corner); (B) geological sketch map showing several bended sheets (horses) of chert and siliceous mudstone, that compose an overturned duplex, Inuyama area, Mino terrane, Japan (modified from Matsuda and Isozaki, 1991; Hori, 1992); (C) a reconstruction of the initial Inuyama duplex showing several OPS "horses" successively thrust under each other (S. Maruyama's interpretation).

for Site III, 433 Ma, 442 Ma and 452 Ma for Site IV, and 443 Ma and 453 Ma for Site V (Fig. 13). All these facts suggest that the direction of subduction was to the NNW and NW in modern coordinates and in respect to the present-day distribution of geological features (Fig. 17; section 5). Vice versa, in the eastern part of the Itmurundy Zone, the MDA of the sandstone from the northern fold (Fig. 3), is younger than that of the sandstone from the southern fold in Site VII (Fig. 15) suggesting another direction of subduction also in the present-day coordinates (Fig. 17).

In Sites VI and VII, the duplex structures are present as well but could be overturned during later collisional processes (Fig. 19A). Such overturned duplexes are similar to that reconstructed in details in the OPS type locality in Japan, the Mino terrain (Fig. 19B) (Matsuda and Isozaki, 1991; Hori, 1992; Safonova et al., 2016, 2020). These two folds in Sites VI and VII represent overturned duplexes (Figs. 3 and 19A), similar to those of the famous Inuyama area (OPS type locality) of the Mino terrain in Japan (Fig. 19B). If we "unfold" them to an of initial position, we will get a direction to approximately south-east (Fig. 19A). Such an approach was previously used at to show several horses thrust under each other and forming a duplex structure (Fig. 19B, C). In addition, so far, we have diagnosed MORB-type basalts only in Site VI. We propose that initially the Type 1 and Type 2 OPS units (Sites I–V) and Type 3 OPS units (Sites VI–VII) were separated from each other by a mid-oceanic ridge (Figs. 17 and 20). According to the paleomagnetic data from the Arkharsu Massif (Fig. 3), a nearly 2000 km long submeridional mid-oceanic ridge extended from the equator to 20°N (Didenko et al., 1994; Kurenkov et al., 2002). Thus, we argue about the presence of pieces of two oceanic plates in the Itmurundy Zone, which were subducting in different directions.

9. A new tectonic model

The Kazakh Paleozoides include many supra-subduction complexes or zones (Fig. 2B), both intra-oceanic and continental, suggesting a continuous subduction from the Cam-

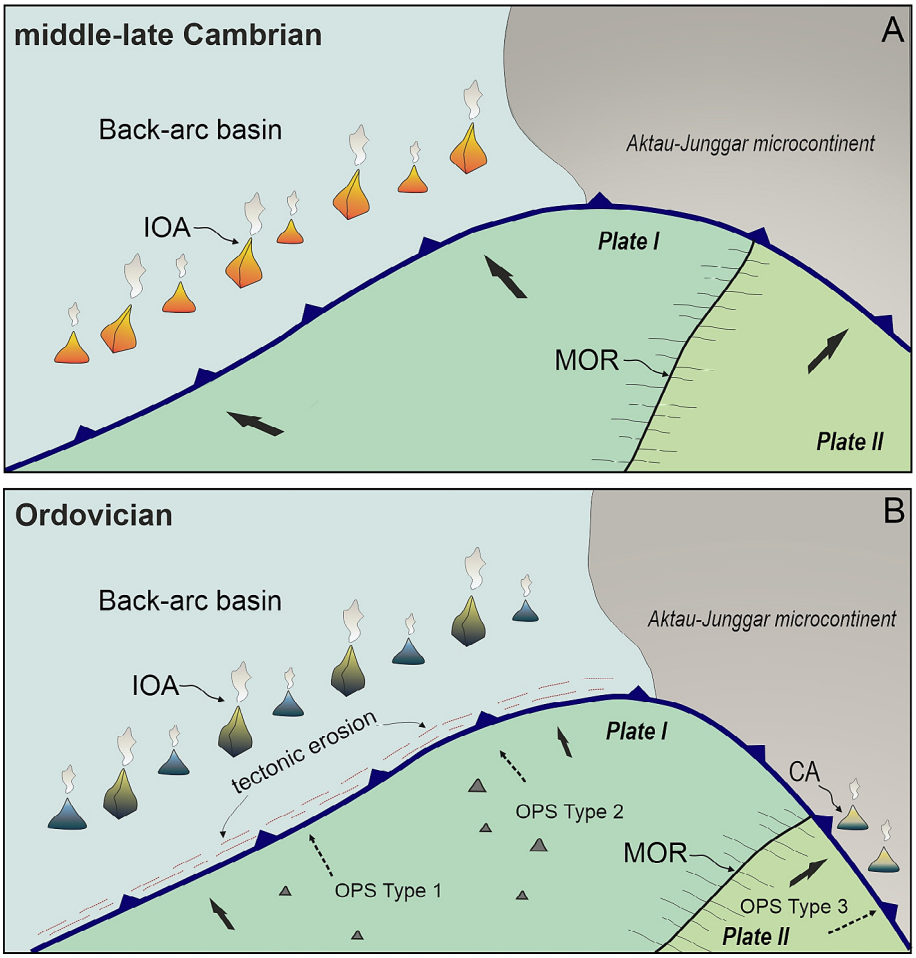

Fig. 20. A new tectonic model for the establishment of the Itmurundy Zone suggesting two oceanic plates, that were once co-existing near the Aktau-Junggar microcontinent and subducting in different directions under different types of convergent margins: Aleutian-type (A; middle-late Cambrian) and Cordilleran-type (B; Ordovician).

brian to the Devonian (e.g., Windley et al., 2007; Degtyarev, 2012; Safonova et al., 2017). Among the early Paleozoic arcs, the largest is the middle-late Cambrian Boshchekul-Chingiz intra-oceanic arc, that is extended from central Kazakhstan to NW China (Degtyarev, 2011; Shen et al., 2015). There are also early Paleozoic island-arc complexes in West Junggar, NW China (e.g., Xu et al., 2013; Zheng et al., 2019; Liao et al., 2021), and south Kazakhstan to northern Tianshan, Kyrgyzstan (Alexeiev et al., 2011; Degtyarev, 2011). Fragments of late Cambrian and Early Ordovician intra-oceanic arcs were also found in the Itmurundy and Tekturmas zones of central Kazakhstan and in the Tangbale accretionary complexes of West Junggar (Figs. 3 and 19), but present only as small incoherent bodies or blocks in serpentinite/ophiolitic mélange (e.g., Zhang et al., 2018; Khassen et al., 2020; Safonova et al., 2020; Degtyarev et al., 2021a, b; Liao et al., 2021).

More records of the occurrence of intra-oceanic arcs in the western PAO come from the clastic rocks, sandstones, often present as turbidites, in the Itmurundy (Sites I–V), Tekturmas and Tangbale ACs (Choulet et al., 2012; Perfilova et al., 2022; Safonova et al., 2022; Safonova and Perfilova, 2023). The sandstones/turbidites could be deposited in the trench, fore-arc, intra-arc and back-arc basins. The U–Pb detrital zircon age patterns, that were obtained from sandstones of these three accretionary complexes, are all unimodal and show main peaks at the Ordovician. This confirms the existence of a long-lived and extended intra-oceanic arc system in the western PAO (Fig. 20), which erosion supplied mafic to andesitic isotopically juvenile material to the trench/forearc basin. The U–Pb zircon data from Sites VI-VII indicate a coeval continental arc (Fig. 8A–D), which destruction provided more felsic and isotopically recycled material (sections 4.3 and 8). The U–Pb zircon age constraints fit those obtained from microfossils in pelagic cherts (Fig. 18, Table 1; Supplementary Data Table S1). The Itmurundy AC records the accretion at the intra-oceanic convergent margin (Fig. 17) during about 50 Myr (section 8), whereas at the continental margin it was much shorter (less 8 Ma), suggesting that the first oceanic plate was larger than the second (Fig. 20).

So, the Types 1 and 2 OPS successions were formed on an oceanic plate subducting under one or more intra-oceanic arcs (Izu-Bonin-Mariana or Aleutian types). The Type 3 OPS rocks were deposited on an oceanic plate moving in another direction probably under a continental arc or active continental margins (Cordilleran or Andean types) (Fig. 20). Such a tectonic setting resembles that in the modern Pacific. The most appropriate actualistic analogue of such tectonic settings are the Aleutian arc, which formed over the Pacific Plate subducting to the north and is characterized by active processes of subduction erosion (Jicha and Key, 2018), and the proto-Juan-de-Fuca Plate subducting under the Northern Cordilleran active margin at 20 Ma (e.g., Madsen et al., 2006). Both plates, Pacific and Juan-de-Fuca, are subducting beneath the North American continent; the directions of their subduction are to the north-northeast and east, respectively. In the tectonic framework of early Paleozoic continental blocks and island arc of the western PAO, we can suggest that the proposed oceanic plates were subducting under the active margins of the

Aktau-Junggar ribbon microcontinent (Fig. 20) (e.g., Windley et al., 2007; Alexeiev et al., 2011; Wilhem et al., 2012) or under the Aktau-Mointy microcontinent located to the north or the Aktau-Junggar microcontinent located to the south-east of the Itmurundy Zone (Fig. 2) (e.g., Levashova et al., 2010; Kanygina et al., 2020).

The proposed model suggests ridge subduction (Fig. 20). Although it is hard to get evidence of ridge subduction while studying fossil Pacific-type orogenic belts, we used the criteria for that from the modern Circum-Pacific. The Itmurundy Zone carries typical signatures of ridge subduction (Wang et al., 2020), which are the great variety of igneous rocks, first of all, high-Mg andesites, boninites, adakites (Safonova et al., 2020; Degtyarev et al., 2021a), enhanced subduction erosion (Safonova et al., 2022; Safonova and Perfilova, 2023; see section 10 below), and the abundant Ordovician–early Devonian gold and copper mineralization (Kurchavov et al., 2002; Seltmann et al., 2009; Goldfarb et al., 2014; Shen et al., 2018). In general, the ridge subduction could result in the splitting of a larger Ordovician oceanic plate into two smaller plates (microplates) like was proposed for the Farallon Plate, which, due to the subduction of the Pacific-Farallon Ridge, became smaller and finally split into the Juan de Fuca and South Farallon plates (Li et al., 2018b, 2022, 2023). However, more detailed research is needed to provide a robust evidence for the ridge subduction and related magmatism, subduction erosion and mineralization in the North-Balkhash foldbelt.

10. The problem of subduction erosion

The most challengeable issue of the reconstruction of both intra-oceanic and continental arcs is a probable disappearance of those arcs, in particular, their igneous formations, from the geological record due to surface and subduction erosion (e.g., Clift and Vanucchi, 2004; Stern and Scholl, 2010; Stern, 2011; Vanucchi et al., 2016; Safonova, 2017; Safonova and Khanchuk, 2021; Safonova and Perfilova, 2023). The relief of oceanic floor is an important factor of subduction erosion. Horst-graben topography of the subducting oceanic plate, an orthogonal subduction of intra-oceanic arcs and ridges and accretion of oceanic rises (seamounts) - all enhance the subduction erosion of magmatic arcs and re-accretion of previously accreted OPS units (von Huene and Ranero, 2003; Martínez-Loriente et al., 2019). Evidence for the subduction erosion comes from the proximity of coeval accretionary and supra-subduction complexes, presence of supra-subduction igneous rocks as blocks in exhumed serpentinite mélange, trench jumping landward and related, magmatic lulls and the disappearance of U–Pb zircon age peaks in younger clastic rocks.

In the Itmurundy and Tekturmas zones of Central Kazakhstan (Safonova et al., 2020, 2022; Gurova et al., 2022) and in the Tangbale-Mayile-Barleik arc belt in West Junggar (e.g., Xu et al., 2013; Zhu et al., 2015; Zheng et al., 2019), the accreted OPS units are located very close to the coeval supra-subduction complexes. This suggests that a part of the crust between them was eroded (Scholl and von Huene, 2007; Safonova et al., 2015). In all these regions, the middle-late Cambrian igneous rocks of supra-subduction origin have been diagnosed only as blocks in serpentinite mélange. There are few Cambrian ages among the detrital zircons from greywacke sandstones of these belts (Choulet et al., 2012; Safonova et al., 2022; Safonova and Perfilova, 2023). In addition, the Cambrian age peak in an older Tekturmas sandstone disappeared in a younger sandstone (Perfilova et al., 2022). All these facts allow us to propose that the Cambrian magmatic arc was tectonically eroded and its fragments (plagiogranite and diorite) were detached from the hanging wall of the subduction zone and captured by the serpentinite formed in the subduction channel and later exhumed (Fig. 20) (Safonova and Perfilova, 2023). Therefore, the processes of subduction erosion in the western PAO were similar to those in the modern Circum-Pacific, for example, over the Guatemala-Costa Rica-Chile (eastern Pacific), Tonga (SW Pacific) and Nankai-Japan (western Pacific) subduction zones (von Huene and Ranero, 2003; Bangs et al., 2006; Contreras-Reyes et al., 2011).

11. Conclusions

The Itmurundy Zone of Central Kazakhstan is a typical Pacific-type orogenic belt hosting accretionary complex, ophiolite massifs and serpentinite mélange. The available geological, U–Pb age, microfossil, geochemical and isotope data from igneous rocks, deep-sea sediments and greywacke sandstones and the new geological and geochronological data prove the existence of two intra-oceanic arcs and two oceanic plates in the western Paleo-Asian Ocean in early Paleozoic time, middle-late Cambrian and Ordovician. We used the Ocean Plate Stratigraphy (OPS) model to trace the evolution of the Itmurundy Zone and to present a holistic story of Ordovician oceanic plates, which accretion formed the Itmurundy accretionary complex. The results of our detailed mapping in seven sites in the western (I, II), central (III–V) and eastern (VI, VII) parts of the Itmurundy Zone allowed us to distinguish three types of OPS assemblages: (1) Chert-dominated, (2) OIB-hosting, and (3) MORB-hosting. The accretion of OPS Types 1 and 3 formed typical accretionary prisms, but accretion of OPS Type 2 formed a more chaotic complex or accretionary mélange. The greywacke sandstones from the western and central parts of the Itmurundy Zone appeared different from those of the eastern part in composition and the character of U–Pb age spectra. The sandstones of OPS Types 1 and 2 show chemical compositions close to basalt to andesite, positive values of whole-rock $\varepsilon_{Nd}(t)$ and $\varepsilon_{Hf}(t)$-in-zircon and unimodal distributions of U–Pb zircon ages with main peaks of magmatism at 460–455 Ma, and MDA of 455 Ma to 433 Ma. The sandstones of OPS Type 3 show chemical compositions close to andesite to dacite, negative values of whole-rock $\varepsilon_{Nd}(t)$, negative to positive values of $\varepsilon_{Hf}(t)$-in-zircon and polymodal distributions of U–Pb zircon ages with the magmatism peaked at ca. 460 Ma and MDA of 459 Ma to 452 Ma. In general, the U–Pb ages of detrital zircons from greywacke sandstones traces the magmatism in the provenance from the Early to the Late Ordovician. The arrival times for the oceanic plate(s) were, respectively, 490 Ma, 475 Ma and 465 Ma. The MDA of sandstones and the microfossils data from chert show the younging of strata to the south and SE in Types 1 and 2 and to NEE for Type 3 (in present coordinates) suggesting double-sided subduction to the NNW and SEE and, accordingly, the co-existence of two oceanic plates in Ordovician time. Those two oceanic plates were subducting under different types of Pacific-type convergent margins, intra-oceanic arc and continental arc. A probable actualistic example is the Aleutian arc with the Pacific Plate subducting to the north and the Juan-de-Fuca Plate back to 20 Ma subducting to the west and WWS under the Cordilleran active margin. The U–Pb zircon data from both igneous and clastic rocks revealed traces of a middle-late Cambrian intra-oceanic arc, which was tectonically eroded during the Early Ordovician subduction. The Cambrian arc was tectonically eroded probably by the relief of the oceanic floor and its oblique position in respect to the subduction zone. As a whole, the Itmurundy AC records the timing of subduction and accretion from the late Cambrian to the early Silurian, i.e., 60 Myr at shortest.

CRediT authorship contribution statement

Inna Safonova: Funding acquisition, Conceptualization, Supervision, Validation, Writing – original draft, Writing – review & edit-

ing. **Ilya Savinskiy:** Investigation, Data curation, Formal analysis, Methodology, Writing – original draft. **Alina Perfilova:** Conceptualization, Data curation, Investigation, Methodology, Validation, Writing – review & editing. **Olga Obut:** Validation, Methodology, Writing – review & editing. **Alexandra Gurova:** Validation, Methodology, Writing – review & editing. **Sergei Krivonogov:** Validation, Writing – review & editing.

Declaration of competing interest

The authors declare that they have no known competing financial interests or personal relationships that could have appeared to influence the work reported in this paper.

Acknowledgements

We appreciate mutual discussions about the Itmurundy Zone with RAS Academician K. Degtyarev, RAS Corr. Member A. Didenko, Drs. Yakubchuk and D. Alexeiev and help with fieldwork from Drs. S. Khromykh, P. Kotler, Mr. D. Pecherichenko and O. Gerasimov. The study was supported by the Russian Science Foundation (#21-77-20022; stratigraphy, geochronology, geochemistry), Fundamental Research Funds for the Central Universities of China (2682023CX016, paper preparation), and Ministry of Science and Higher Education of Russia, State Assignment Projects (122041400044-2 and FSUS-2020-0039) (petrography, isotopes, geodynamic implications).

Appendix A. Supplementary data

Supplementary data to this article can be found online at https://doi.org/10.1016/j.gsf.2024.101814.

References

Abrajevitch, A.V., Van der Voo, R., Bazhenov, M.L., Levashova, N.M., McCausland, P.J. A., 2008. The role of the Kazakhstan orocline in the late Paleozoic amalgamation of Eurasia. Tectonophysics 455, 61–76.

Ackerman, L., Hajna, J., Žák, J., Erban, V., Sláma, J., Polák, L., Kachlík, V., Strnad, L., Trubač, J., 2019. Architecture and composition of ocean floor subducted beneath northern Gondwana during Neoproterozoic to Cambrian: a palinspastic reconstruction based on Ocean Plate Stratigraphy (OPS). Gondwana Res. 76, 77–97.

Alexeiev, D.V., Ryazantsev, A.V., Kröner, A., Tretyakov, A.A., Xia, X., Liu, D.Y., 2011. Geochemical data and zircon ages for rocks in a high-pressure belt of Chu-Yili Mountains, southern Kazakhstan: implications for the earliest stages of accretion in Kazakhstan and the Tianshan. J. Asian Earth Sci. 42 (5), 805–820.

Ando, H., Tomosugi, T., Kanakubo, T., 2001. Upper Cretaceous to Paleocene Hakobuchi Group, Nakatonbetsu area, northern Hokkaido – lithostratigraphy and megafossil biostratigraphy. J. Geol. Soc. Japan 107, 142–162.

Antonyuk, R.M., 1974. Oceanic crust of the eugeosynclinal region of east Central Kazakhstan. Tectonics of the Ural-Mongolian Fold Belt, Moscow (in Russian).

Avdeev, A.V., 1986. Geology of ophiolitic zones of Kazakhstan. Abs. Diss., Novosibirsk, 32p. (in Russian).

Bangs, N.L.B., Gulick, S.P.S., Shipley, T.H., 2006. Seamount subduction erosion in the Nankai trough and its potential impact on the seismogenic zone. Geology 34, 701–704.

Bazhenov, M.L., Levashova, N.M., Degtyarev, K.E., Van der Voo, R., Abrajevitch, A.V., McCausland, P.J.A., 2012. Unraveling the early–middle Paleozoic paleogeography of Kazakhstan on the basis of Ordovician and Devonian paleomagnetic results. Gondwana Res. 22, 974–991.

Berzin, N.A., Dobretsov, N.L., 1994. Geodynamic evolution of southern Siberia in Late Precambrian-Early Paleozoic time. In: Coleman, R.G. (Ed.), Reconstruction of the Paleo-Asian Ocean. VSP International Sciences Publishers, Utrecht, The Netherlands, pp. 53–70.

Bespalov, V.F., 1956. Middle Paleozoic Dzhungar-Balkhash intrageosyncline. Soviet Geology 52p.. in Russian).

Bhatia, M.R., 1983. Plate tectonics and geochemical composition of sandstone. J. Geol. 91, 611–627.

Briqueu, L., Bougault, H., Joron, J.L., 1984. Quantification of Nb, Ta, Ti and V anomalies in magmas associated with subduction zones: petrogenetic implications. Earth Planet. Sci. Lett. 68 (2), 297–308.

Buslov, M.M., 2011. Tectonics and geodynamics of the Central Asian fold belt: the role of Late Paleozoic large-amplitude strike-slip faults. Rus. Geol. Geoph. 52 (1), 52–71.

Buslov, M.M., Saphonova, I.Y., Watanabe, T., Obut, O.T., Fujiwara, Y., Iwata, K., Semakov, N.N., Sugai, Y., Smirnova, L.V., Kazansky, A.Y., 2001. Evolution of the Paleo-Asian Ocean (Altai–Sayan region, Central Asia) and collision of possible Gondwana-derived terranes with the southern marginal part of the Siberian continent. Geosci. J. 5, 203–224.

Chen, C.-Y., Frey, F.A., Garcia, M.O., Dalrymple, G.B., Hart, S.R., 1991. The tholeiitic to alkaline basalt transition at Heleakala volcano Maui, Hawaii. Contrib. Mineral. Petrol. 106, 183–200.

Choulet, F., Chen, Y., Wang, B., Faure, M., Cluzel, D., Charvet, J., Xu, B., 2011. Late Paleozoic paleogeographic reconstruction of Western Central Asia based upon paleomagnetic data and its geodynamic implications. J. Asian Earth Sci. 42 (5), 867–884.

Choulet, F., Faure, M., Cluzel, D., Chen, Y., Lin, W., Wang, B., 2012. From oblique accretion to transpression in the evolution of the Altaid collage: new insights from West Junggar, northwestern China. Gondwana Res. 21, 530–547.

Clift, P., Vanucchi, P., 2004. Controls on tectonic accretion versus erosion in subduction zones: implications for the origin and recycling of the continental crust. Rev. Geophys. 42 (2), RG2001.

Contreras-Reyes, E., Grevemeyer, I., Watts, A.B., Flueh, E.R., Peirce, C., Moeller, S., Papenberg, C., 2011. Deep seismic structure of the Tonga subduction zone: implications for mantle hydration, tectonic erosion, and arc magmatism. J. Geophys. Res. 116, B10103.

Cox, R., Lowe, D.R., 1995. A conceptual review of regional-scale controls on the composition of clastic sediment and the co-evolution of continental blocks and their sedimentary cover. J. Sed. Res. 1, 1–12.

Dagva-Ochir, L., Oyunchimeg, T.-U., Enkhdalai, B., Safonova, I., Li, H., Otgonbaatar, D., Tamehe, L.S., Sharav, D., 2020. Middle Paleozoic intermediate-mafic rocks of the Tsoroidog Uul' accretionary complex, Central Mongolia: petrogenesis and tectonic implications. Lithos 376–377, 105795.

Degtyarev, K.E., 1999. Tectonic evolution of the early Paleozoic active margin in Kazakhstan. Moscow, Nauka,. 123 p. (in Russian).

Degtyarev, K.E., 2011. Tectonic evolution of Early Paleozoic island-arc systems and continental crust formation in the Caledonides of Kazakhstan and the North Tien Shan. Geotectonics 45 (1), 23–50.

Degtyarev, K.E., Ryazantsev, A.V., 2007. Model of the Cambrian arc–continent collision for the paleozoids of Kazakhstan. Geotectonics 1, 71–96. in Russian).

Degtyarev, K.E., Tolmacheva, T.Y., Tretyakov, A.A., Kotov, A.B., Yakubchuk, A.S., Salnikova, E.B., Wang, K.-L., 2017. Polychronous formation of the ophiolite association in the Tekturmas zone of Central Kazakhstan inferred from geochronological and biostratigraphic data. Doklady Earth Sci. 472, 26–30.

Degtyarev, K.E., Tolmacheva, T.Y., Tretyakov, A.A., 2020. Siliceous–volcanic associations of the Northern Balkhash ophiolite zone (Central Kazakhstan): biostratigraphy, sedimentation and tectonic evolution in the Middle-Late Ordovician. Palaeogeogr. Palaeocl. Palaeoecol. 551, 109748.

Degtyarev, K.E., Luchitskaya, M.V., Tretyakov, A.A., Pilitsyna, A.V., Yakubchuk, A.S., 2021a. Early Paleozoic suprasubduction complexes of the North Balkhash ophiolite zone (Central Kazakhstan): geochronology, geochemistry and implications for tectonic evolution of the Junggar-Balkhash Ocean. Lithos 380–381, 105818.

Degtyarev, K., Yakubchuk, A.S., Luchitskaya, M.V., Tolmacheva, T.Y., Skoblenko (Pilitsyna), A.V., Tretyakov, A.A., 2021b. Ordovician supra-subduction, oceanic and within-plate ocean island complexes in the Tekturmas ophiolite zone (Central Kazakhstan): age, geochemistry and tectonic implications. Int. Geol. Rev. 64 (15), 2108–2150.

Degtyarev, K.E., 2012. Tectonic Evolution of the Early Paleozoic Island Arc Systems and Formation of the Continental Crust in the Caledonides of Kazakhstan. GEOS, Moscow, p. 2012 (in Russian).

Dewey, J.F., Bird, J.M., 1970. Mountain belts and the new global tectonics. J. Geophys. Res. 75, 2625–2647.

Dickinson, W.R., Beard, L.S., Brakenridge, G.R., Erjavec, J.L., Ferguson, R.C., Inman, K. F., Knepp, R.A., Lindberg, F.A., Ryberg, P.T., 1983. Provenance of North American Phanerozoic sandstones in relation to tectonic setting. Geol. Soc. Am. Bull. 94 (2), 222–235.

Didenko, A., Mossakovsky, A., Pechersky, D., Ruzhentsev, S., Samygin, S., Kheraskova, T., 1994. Geodynamics of Paleozoic oceans of Central Asia. Geol. Geofiz. 35 (7–8), 59–75 (in Russian).

Dobretsov, N.L., Berzin, N.A., Buslov, M.M., 1995. Opening and tectonic evolution of the paleo-Asian Ocean. Int. Geol. Rev. 37, 335–360.

Dobretsov, N.L., Buslov, M.M., Safoшova, I.Y., Kokh, D.A., 2004. Fragments of oceanic island in the Kurai and Katun' accretionary wedges of Gorny Altai. Russ. Geol. Geophys. 45 (12), 1381–1403.

Eizenhöfer, P.R., Zhao, G., Zhang, J., Sun, M., 2014. Final closure of the Paleo-Asian Ocean along the Solonker Suture Zone: constraints from geochronological and geochemical data of Permian volcanic and sedimentary rocks. Tectonics 33 (4), 441–463.

Ermolov, P.V., 2008. A new look at the origin of the ophiolite belts of Kazakhstan. Izvestia NAN RK, Seria Geologic'eskaya 1, 76–85 (in Russian).

Ermolov, P.V., Stepanets, V.G., Sentov, N., 1990. Ophiolites of Kazakhstan. Guide of the excursion of the international workshop on the project No. 2 "Ophiolites. UT "Offset", Karaganda, 67p. (in Russian).

Esenov, S.E., Lyapichev, G.F., Shlygin, E.D., Avdeev, A.V., 1972. Geology of the USSR. volume XX. Central Kazakhstan. Geological Description. Book 2. Moscow "Nedra", 380 p. (in Russian).

Feng, R., Kerrich, R., 1990. Geochemistry of fine grained clastic sediments in the Archaean Abitibi Greenstone Belt, Canada: implications for provenance and tectonic setting. Geochim. Cosmochim. Acta 54, 1061–1081.
Filippova, I.B., Bush, V.A., Didenko, A.N., 2001. Middle Paleozoic subduction belts: the leading factor in the formation of the Central Asian fold-and-thrust belt. Russ. J. Earth. Sci. 3 (6), 405–426.
Fryer, P., 2012. Serpentinite mud volcanism: observations, processes, and implications. Annu. Rev. Mar. Sci. 4, 345–373.
Fujioka, K., Tanaka, T., Aoike, K., 1995. Serpentine seamount in Izu-Bonin and Mariana forearcs: observation by a submersible and its relation to onland serpentinite belt. J. Geog. 104 (3), 473–494.
Goldfarb, R.J., Taylor, R.D., Collins, G.S., Goryachev, N.A., Orlandini, O.F., 2014. Phanerozoic continental growth and gold metallogeny of Asia. Gondwana Res. 25, 48–102.
Grishin, D.V., Pechersky, D.M., Degtyarev, K.E., 1997. Paleomagnetic reconstruction of the Middle Paleozoic structure of Central Kazakhstan. Geotectonics 31 (1), 65–75.
Gurova, A.V., Safonova, I.Y., Savinsky, I.A., Antonyuk, R.M., Orynbek, T.Z., 2022. Magmatic rocks of the Tekturmass accretionary complex, Central Kazakhstan: geological position and geodynamic settings of formation. Geodyn. Tectonophys. 13 (5), 0673.
Heinhorst, J., Lehmann, B., Ermolov, P., Serykh, V., Zhurutin, S., 2000. Paleozoic crustal growth and metallogeny of Central Asia: evidence from magmatic-hydrothermal ore systems of Central Kazakhstan. Tectonophysics 328, 69–87.
Hori, R., 1992. Radiolarian biostratigraphy at the Triassic/Jurassic period boundary in bedded cherts from the Inuyama Area, Central Japan. J. Geosci. 35, 53–65.
Hori, N., Wakita, K., 2004. Reconstructed oceanic plate stratigraphy of the Ino Formation in the Ino district, Kochi prefecture, Central Shikoku, Japan. J. Asian Earth Sci. 24 (2), 185–197.
Huneke, H., Henrich, R., 2011. Pelagic sedimentation in modern and ancient oceans. Dev. Sedimentol. 63, 215–351.
Isozaki, Y., Maruyama, S., Fukuoka, F., 1990. Accreted oceanic materials in Japan. Tectonophysics 181, 179–205.
Jiang, Y.D., Schulmann, K., Kröner, A., Sun, M., Lexa, O., Janoušek, V., Hanžl, P., 2017. Neoproterozoic-early Paleozoic peri-Pacific accretionary evolution of the Mongolian collage system: insights from geochemical and U-pb zircon data from the Ordovician sedimentary wedge in the Mongolian Altai. Tectonics 36 (11), 2305–2331.
Jicha, B., Key, S.M., 2018. Quantifying arc migration and the role of forearc subduction erosion in the central Aleutians. J. Volcanol. Geotherm. Res. 360, 84–99.
Johnson, L.E., Fryer, P., 1990. The first evidence of MORB-like lavas on the Mariana forearc: geochemistry, petrology and implications for tectonic evolution. Earth Planet. Sci. Lett. 100 (1), 304–316.
Kanygina, N., Tretyakov, A., Degtyarev, K.E., Lee, H.-Y., 2020. Quartzite-schist sequences of the Aktau-Mointy Massif (Central Kazakhstan): structural position, provenance, and formation stages of the Earth crust in the Precambrian. Geotectonics 54 (2), 212–228.
Kemkin, I.V., Khanchuk, A.I., 1994. Jurassic accretionary prism in the southern Sikhote-Alin. Geol. Pac. Ocean 10, 831–839.
Kemkin, I.V., Khanchuk, A.I., Kemkina, R.A., 2016. Accretionary prisms of the Sikhote-Alin orogenic belt: composition, structure and significance for reconstruction of the geodynamic evolution of the eastern Asian margin. J. Geodyn. 102, 202–230.
Kerr, A.C., White, R.V., Saunders, A.D., 2000. LIP reading: recognizing oceanic plateaus in the geological record. J. Petrol. 41, 1041–1056.
Khanchuk, A.I., 1993. Geological structure and development of the continental frame of the Pacific northwest. Abs. diss. Dr. geol.-min. sci., Moscow 31.
Khassen, B.P., Safonova, I.Y., Yermolov, P.V., Antonyuk, R.M., Gurova, A.V., Obut, O.T., Perfilova, A.A., Savinskiy, I.A., Tsujimori, T., 2020. The Tekturmas ophiolite belt of Central Kazakhstan: geology, magmatism, and tectonics. Geol. J. 55 (3), 2363–2382.
Kimura, G., Mukai, A., 1991. Underplated units in an accretionary complex: melange of the Shimanto belt of eastern Shikoku, Southwest Japan. Tectonics 10 (1), 31–50.
Knittel, U., Walia, M., Suzuki, S., Lee, Y.-H., Takesue, N., Lee, H.-Y., 2020. U-pb ages and hf isotope composition of zircon from the Shimanto accretionary complex: evidence for heterogeneous sources. Geochem. J. 54 (5), 277–288.
Kojima, S., Tsukada, K., Otoh, S., Yamakita, S., Ehiro, M., Dia, C., Kirillova, G.L., Dymovich, V.A., Eichwald, L.P., 2008. Geological relationship between Anyui metamorphic complex and Samarka terrane, Far East Russia. Isl. Arc 17, 502–516.
Korobkin, V.V., 2011. Tectonic zonation and structural styles of Paleozoids of Kazakhstan. Izvestiya Tomskogo Politekhnicheskogo Universiteta 319 (1), 71–77 (in Russian).
Koshkin, V.Y., Abdrahmanov, B.M., Volkov, V.V., Mertenov, V.M., 1987. Stratigraphy of the Ordovician and Silurian terrigenous-siliceous-basalt formation of the northern Balkhash region. Regional Geology and Geophysics of Kazakhstan, Alma-Ata, KazIMS, 159 p. (in Russian).
Koshkin, V.Y., Galitsky, V.V., 1960. Geological map of the USSR. 1: 200 000. Series Balkhash. Sheet L-43-XI. South Kazakhstan Geological Department of the Ministry of Geology and Mineral Protection of the USSR (in Russian).
Kovalenko, V.I., Yarmolyuk, V.V., Kovach, V.P., Kotov, A.B., Kozakov, I.K., Salnikova, E. B., Larin, A.M., 2004. Isotope provinces, mechanisms of generation and sources of the continental crust in the Central Asian mobile belt: geological and isotopic evidence. J. Asian Earth Sci. 23, 605–627.
Kröner, A., Kovach, V., Belousova, E., Hegner, E., Armstrong, R., Dolgopolova, A., Seltmann, R., Alexeiev, D.V., Hofmann, J.E., Wong, J., Sun, M., Cai, K., Wang, T., Tong, Y., Wilde, S.A., Degtyarev, K.E., Rytsk, E., 2014. Reassessment of continental growth during the accretionary history of the Central Asian Orogenic Belt. Gondwana Res. 25, 103–125.
Kuramoto, S., Taira, A., Bangs, N.L., Shipley, T.H., Moore, G.F., 2000. Seismogenic zone in the Nankai accretionary wedge general summary of Japan-U.S. collaborative 3-D seismic investigation. J. Geogr. 109, 531–539.
Kurchavov, A.M., Grankin, M.S., Mal'chenko, E.G., Khamzin, B.S., Zhukovskii, V.I., 2002. Metallogenic zonality of the Devonian volcanoplutonic belt in Central Kazakhstan. Geol. Ore Depos. 2002, 18–25.
Kurenkov, S.A., Didenko, A.N., Simonov, V.A., 2002. Geodynamics of Paleospreading. GEOS, Moscow, 294 p. (in Russian).
Kusky, T., Windley, B., Safonova, I., Wakita, K., Wakabayashi, J., Polat, A., Santosh, M., 2013. Recognition of ocean plate stratigraphy in accretionary orogens through Earth history: a record of 3.8 billion years of sea floor spreading, subduction, and accretion. Gondwana Res. 24, 501–547.
Levashova, N.M., Degtyarev, K.E., Bazhenov, M.L., Collins, A.Q., Van der Voo, R., 2003. Permian palaeomagnetism of East Kazakhstan and the amalgamation of Eurasia. Geophys. J. Int. 152, 677–687.
Levashova, N.M., Meert, J.G., Gibsher, A.S., Grice, W.C., Bazhenov, M.L., 2010. The origin of microcontinents in the Central Asian Orogenic Belt: constraints from paleomagnetism and geochronology. Precambr. Res. 185 (1–2), 37–54.
Levashova, N.M., Degtyarev, K.E., Bazhenov, M.L., 2012. Oroclinal bending of the Middle and Late Paleozoic volcanic belts in Kazakhstan: paleomagnetic evidence and geological implications. Geotectonics 46 (4), 285–302.
Li, J.-Y., 2006. Permian geodynamic setting of Northeast China and adjacent regions: closure of the paleo-Asian Ocean and subduction of the paleo-Pacific plate. J. Asian Earth Sci. 26 (3–4), 207–224.
Li, P., Sun, M., Rosenbaum, G., Yuan, C., Safonova, I., Cai, K., Jiang, Y., Zhang, Y., 2018a. Geometry, kinematics and tectonic models of the Kazakhstan orocline, Central Asian Orogenic Belt. J. Asian Earth Sci. 153, 42–56.
Li, S., Suo, Y., Li, X., Liu, B., Dai, L., Wang, G., Zhou, J., Li, Y., Liu, Y., Cao, X., Somerville, I., Mu, D., Zhao, S., Liu, J., Meng, F., Zhen, L., Zhao, L., Zhu, J., Yu, S., Liu, Y., Zhang, G., 2018b. Microplate tectonics: new insights from micro-blocks in the global oceans, continental margins and deep mantle. Earth Sci. Rev. 185, 1029–1064.
Li, S., Suo, Y., Zhou, J., Zhong, S., Sun, G., Liu, J., Wang, G., Zhu, J., Jiang, S., Li, X., Guo, X., Liu, Y., Cao, X., Guo, L., Zhao, S., Wang, P., Guan, Q., Chen, L., Liu, B., Zhou, J., Jiang, Z., Liu, L., Cao, H., Dai, L., Yu, S., Liu, B., Wang, X., Wang, C., Wang, X., Liu, Z., Guan, H., Li, X., Hu, J., Duan, W., Yu, L., Liu, X., Wang, Y., Zhong, Y., Liu, P., Zhang, W., Li, L., Zhao, Y., Xu, S., 2022. Microplate and megaplate: fundamental principles and paradigm transition. Acta Geol. Sinica 96 (10), 3541–3558 (in Chinese).
Li, S., Suo, Y., Zhou, J., 2023. Microplate tectonics: a new tectonic paradigm. Leibniz Online 51, 1–10.
Liao, W., Han, B.-F., Xu, Y., Li, A., 2021. Ediacaran initial subduction and Cambrian slab rollback of the Junggar Ocean: new evidence from igneous tectonic blocks and gabbro enclave in Early Palaeozoic accretionary complexes, southern West Junggar, NW China. Geol. Mag. 158 (10), 1811–1829.
Long, X., Yuan, C., Sun, M., Safonova, I., Xiao, W., Wang, Y., 2012. Geochemistry and U-Pb detrital zircon dating of Paleozoic graywackes in East Junggar, NW China: insights into subduction–accretion processes in the southern Central Asian Orogenic Belt. Gondwana Res. 21, 637–653.
Lu, L., Qin, Y., Zhang, K.-J., Han, C.-Y., Wei, T., Li, Z.-F., Qu, Z.-H., 2020. Provenance and tectonic settings of the Late Paleozoic sandstones in Central Inner Mongolia, NE China: constraints on the evolution of the southeastern Central Asian Orogenic Belt. Gondwana Res. 77, 111–135.
Madsen, J.K., Thorkelson, D.J., Friedman, R.M., Marshall, D.D., 2006. Cenozoic to Recent plate configurations in the Pacific Basin: ridge subduction and slab window magmatism in western North America. Geosphere 2 (1), 11–34.
Martínez-Loriente, S., Sallarès, V., Ranero, C.R., Ruh, J.B., Barckhausen, U., Grevemeyer, I., Bangs, N., 2019. Influence of incoming plate relief on overriding plate deformation and earthquake nucleation: Cocos ridge subduction (Costa Rica). Tectonics 38, 4360–4377.
Maruyama, S., Safonova, I., 2019. Orogeny and mantle dynamics: role of tectonic erosion and second continent in the mantle transition zone. Novosibirsk State Univ, Novosibirsk.
Maruyama, S., Kawai, T., Windley, B.F., 2010. Ocean plate stratigraphy and its imbrication in an accretionary orogen: the Mona complex, Anglesey-Lleyn, Wales, UK. Geol. Soc. London. Spec. Pub. 338, 55–75.
Maruyama, S., Omori, S., Sensu, H., Kawai, K., Windley, B.F., 2011. Pacific-type orogens: new concepts and variations in space and time from present to past. J. Geogr. 120, 115–223 (in Japanese with English abstract).
Matsuda, T., Isozaki, Y., 1991. Well-documented travel history of Mesozoic pelagic chert in Japan: remote ocean to subduction zone. Tectonics 10, 475–499.
Meschede, M., 1986. A method of discriminating between different types of mid-ocean ridge basalts and continental tholeiites with the Nb-Zr-Y diagram. Chem. Geol. 56 (3–4), 207–218.
Miyashiro, A., 1974. Volcanic rock series in island arcs and active continental margins. Am. J. Sci. 274, 321–355.
Mullen, E.D., 1983. $MnO/TiO_2/P_2O_5$: a minor element discriminant for basaltic rocks of oceanic environments and its implications for petrogenesis. Earth Planet. Sci. Lett. 62, 53–62.
Nakae, S., 2000. Regional correlation of the Jurassic accretionary complex in the Inner Zone of Southwest Japan. Memories of Geological Society of Japan 55, 73–98.

Nesbitt, H.W., Young, G.M., 1982. Early Proterozoic climates and plate motions inferred from major element chemistry of lutites. Nature 299, 715–717.
Nikitin, I.F., 2002. Ordovician siliceous and siliceous-basalt complexes of Kazakhstan. Russ. Geol. Geophys. 43, 512–527.
Novikova, M.Z., Gerasimova, N.A., Dubinina, S.V., 1983. Conodonts from the volcanic-siliceous complex of the Northern Balkhash. Doklady AN SSSR 271, 1449–1451 (in Russian).
Patalakha, F.A., Belyi, V.A., 1981. Ophiolites of the Itmurundy-Kazyk zone. In: Abdulin, A.A., Patalakha, F.A. (Eds.), Ophiolites of Kazakhstan. Nauka, Alma-Ata, pp. 7–102 (in Russian).
Pearce, J.A., 2008. Geochemical fingerprinting of oceanic basalts with applications to ophiolite classification and the search for Archean oceanic crust. Lithos 100, 14–48.
Pearce, J.A., 1982. Trace element characteristics of lavas from destructive plate boundaries, in Thorpe, R.S., ed., Andesites 525–548.
Perfilova, A.A., Safonova, I.Y., Gurova, A.V., Kotler, P.D., Savinskiy, I.A., 2022. Tectonic settings of formation of volcanic and sedimentary rocks of the Itmurundy zone, Central Kazakhstan. Geodyn. Tectonophys. 13 (1), 0572.
Perfilova, A.A., 2023. Age, composition and sources of Paleozoic greywacke sandstones of Central and Eastern Kazakhstan. Dissertation for Candidate of Geological and Mineralogical Sciences, Novosibirsk, IGM SB RAS, 242 p.
Pettijohn, F.J., Potter, P.E., Siever, R., 1972. Sand and Sandstone. Springer, Berlin Heidelberg.
Puchkov, V., 2000. Paleogeodynamics of the South and Central Urals. Dauriya, Ufa, 144 p. (in Russian).
Regelous, M., Hofmann, A.W., Abouchami, W., Galer, S.J.G., 2003. Geochemistry of lavas from the Emperor seamounts, and the geochemical evolution of Hawaiian magmatism from 85 to 42 ma. J. Petrol. 44, 113–140.
Rusakov, M.P., 1933. Geological treatise about near Balkhash region and Balkhash Lake, mineral resources district. Leningrad, Tsvetmetizdat, Moscow (in Russian).
Safonova, I.Y., 2009. Intraplate magmatism and oceanic plate stratigraphy of the Paleo-Asian and Paleo-Pacific oceans from 600 to 140 ma. Ore Geol. Rev. 35, 137–154.
Safonova, I., 2017. Juvenile versus recycled crust in the Central Asian Orogenic Belt: implications from ocean plate stratigraphy, blueschist belts and intra-oceanic arcs. Gondwana Res. 47, 6–27.
Safonova, I.Y., Khanchuk, A.I., 2021. Subduction erosion at pacific-type convergent margins. Russ. J. Pacific Geol. 40 (6), 3–19.
Safonova, I., Maruyama, S., 2014. Asia: a frontier for a future supercontinent Amasia. Int. Geol. Rev. 59, 1051–1071.
Safonova, I.Y., Perfilova, A.A., Obut, O.T., Savinsky, I.A., Cherny, R.I., Petrenko, N.A., Gurova, A.V., Kotler, P.D., Khromykh, S.V., Krivonogov, S.K., Maruyama, S., 2019. Itmurundy accretionary complex (Northern Balkhash): geological structure, stratigraphy and tectonic origin. Russ. J. Pacific Geol. 38, 102–117.
Safonova, I., Perfilova, A., Savinskiy, I., Kotler, P., Sun, M., Wang, B., 2022. Sandstones of the Itmurundy accretionary complex, Central Kazakhstan, as archives of arc magmatism and subduction erosion: evidence from U-Pb zircon ages, geochemistry and Hf-Nd isotopes. Gondwana Res. 111, 35–52.
Safonova, I., Perfilova, A., 2023. Survived and disappeared intra-oceanic arcs of the paleo-Asian Ocean: evidence from Kazakhstan. Natl Sci. Rev. 10 (2), nwac215.
Safonova, I., Santosh, M., 2014. Accretionary complexes in the Asia-Pacific region: tracing archives of ocean plate stratigraphy and tracking mantle plumes. Gondwana Res. 25, 126–158.
Safonova, I., Maruyama, S., Litasov, K., 2015. Generation of hydrous-carbonated plumes in the mantle transition zone linked to tectonic erosion and subduction. Tectonophysics 662, 454–471.
Safonova, I., Maruyama, S., Kojima, S., Komiya, T., Krivonogov, S., Koshida, K., 2016. Recognizing OIB and MORB in accretionary complexes: a new approach based on ocean plate stratigraphy, petrology, and geochemistry. Gondwana Res. 33, 92–114.
Safonova, I., Kotlyarov, A., Krivonogov, S., Xiao, W., 2017. Intra-oceanic arcs of the Paleo-Asian Ocean. Gondwana Res. 50, 167–194.
Safonova, I.Y., Savinsky, I.A., Perfilova, A.A., Gurova, A.V., Maruyama, S., Tsujimori, T., 2020. Itmurundy accretionary complex (Northern Balkhash): geological structure, stratigraphy and tectonic origin. Gondwana Res. 79, 49–69.
Sano, H., 1988. Permian oceanic rocks of Mino terrane, Central Japan. J. Geol. Soc. 94, 697–709.
Sano, H., Kanmera, K., 1988. Paleogeographic reconstruction of accreted oceanic rocks, Akiyoshi, Southwest Japan. Geology 16, 600–602.
Savinskiy, I., Safonova, I., Perfilova, A., Kotler, P., Sato, T., Maruyama, S., 2021. A story of Devonian Ocean plate stratigraphy hosted by the Ulaanbaatar accretionary complex, northern Mongolia: implications from geological, structural and U-Pb detrital zircon data. Int. J. Earth Sci. 111, 2469–2492.
Scholl, D., von Huene, R., 2007. Crustal recycling at modern subduction zones applied to the past. Issues of growth and preservation of continental basement crust, mantle geochemistry, and supercontinent reconstruction. In: Hatcher, R. D., Jr., Carlson, M.P., McBride, J.H., Martínez Catalán, J.R. (Eds.), 4-D framework of continental crust. Geol. Soc. Am. Memoir 200, 9–32.
Seltmann R., Shatov V., Yakubchuk A., 2009. Mineral deposits database and thematic maps of Central Asia: London, Natural History Museum, Centre for Russian and Central Eurasian Mineral Studies (CERCAMS), 143 p. and ArcGIS 9.2, ArcView 3.2 and MapInfo 6.0 (7.0) GIS packages, scale 1:1 500 000, CD-ROM.
Sengör, A.M.C., Natal'in, B.A., Burtman, V.S., 1993. Evolution of the Altaid tectonic collage and Paleozoic crustal growth in Eurasia. Nature 364, 299–307.
Shen, P., Pan, H., Seitmuratova, E., Yuan, F., Jakupova, S., 2015. A Cambrian intraoceanic subduction system in the Bozshakol area, Kazakhstan. Lithos 224–225, 61–77.
Shen, P., Pan, H.D., Hattori, K., David, R.C., Seitmuratova, E., 2018. Large paleozoic and mesozoic porphyry deposits in the Central Asian orogenic belt: geodynamic settings, magmatic sources, and genetic models. Gondwana Res. 58, 161–194.
Shutov, V.D., 1967. Classification of sandstones. Lithol. Mineral Resour. 5, 86–102 (in Russian).
Stepanets, W.G., 2016. Ophiolites of Kazakhstan. Geology and Geodynamics. Acad. Pub. House Lambert. 251 (in Russian).
Stern, C.R., 2011. Subduction erosion: rates, mechanisms, and its role in arc magmatism and the evolution of the continental crust and mantle. Gondwana Res. 20, 284–308.
Stern, R.J., Scholl, D.W., 2010. Yin and yang of continental crust creation and destruction by plate tectonic processes. Int. Geol. Rev. 52 (1), 1–31.
Sun, S., McDonough, W.F., 1989. Chemical and isotopic systematics of oceanic basalts: implications for mantle composition and processes. In: Saunders, A.D., Norry, M.J. (Eds.), Magmatism in the Ocean Basins. Geol. Soc. London, Spec. Pub. 42, 313-345.
Sweet, W., Bergstrom, S.M., 1984. Conodont provinces and biofacies of the Late Ordovician. Conodont Biofacies and Provincialism, Geological Society of America, GSA special papers 196, 69 p.
Taylor, S.T., McLennan, S.M., 1985. The Continental Crust: Composition and Evolution. Blackwell, Oxford, p. 312.
Tolmacheva, T.Y., Holmer, L.S., Popov, L.E., Gogin, I.Y., 2004. Conodont biostratigraphy and faunal assemblages in radiolarian ribbon-banded cherts of the Burubaital Formation, West Balkhash Region, Kazakhstan. Geol. Mag. 141 (6), 699–715.
Tolmacheva, T.Y., Degtyarev, K.E., Ryazantsev, A., Nikitina, O.I., 2009. Conodonts from the upper Ordovician siliceous rocks of Central Kazakhstan. Paleontol. J. 43 (11), 1498–1512.
Tolmacheva, T.Y., Degtyarev, K.E., Ryazantsev, A., 2021. Ordovician conodont biostratigraphy, diversity and biogeography in deep-water radiolarian cherts from Kazakhstan. Palaeogeogr. Palaeoclimatol. Palaeoecol. 578, (12) 110572.
Trifonov, V.G., 1967. Late Paleozoic structure of the North Balkhash region and its origin. Moscow, Nauka,. 254 p. (in Russian).
Vanucchi, P., Morgan, J.P., Balestrieri, M.L., 2016. Subduction erosion, and the de-construction of continental crust: the Central America case and its global implications. Gondwana Res. 40, 184–198.
von Huene, R., Ranero, C.R., 2003. Subduction erosion and basal friction along the sediment-starved convergent margin off Antofagasta, Chile. J. Geophys. Res. 108 (B2), 2079.
Wakabayashi, J., 2015. Anatomy of a subduction complex: architecture of the Franciscan Complex, California, at multiple length and timescale. Int. Geol. Rev. 57, 669–746.
Wakita, K., 2012. Mappable features of mélanges derived from ocean plate stratigraphy in the Jurassic accretionary complexes of Mino and Chichibu terranes, Southwest Japan. Tectonophysics 568–569, 74–85.
Wakita, K., 2013. Geology and tectonics of Japanese islands: a review – the key to understanding the geology of Asia. J. Asian Earth Sci. 72, 75–87.
Wakita, K., 2015. OPS mélange: a new term for mélanges of convergent margins of the world. Int. Geol. Rev. 57 (5–8), 1–11.
Wakita, K., Metcalfe, I., 2005. Ocean plate stratigraphy in east and southeast Asia. J. Asian Earth Sci. 24, 679–702.
Wang, B., Faure, M., Shu, L.S., Cluzel, D., Charvet, J., de Jong, K., Chen, Y., 2008. Paleozoic geodynamic evolution of the Yili Block, Western Chinese Tianshan. Bull. Soc. Géol Fr. 179 (5), 483–490.
Wang, B., Jahn, B.M., Shu, L.S., Li, K.S., Chung, S.L., Liu, D.Y., 2012. Middle-Late Ordovician arc-type plutonism in the NW Chinese Tianshan: implication for the accretion of the Kazakhstan continent in Central Asia. J. Asian Earth Sci. 49, 40–53.
Wang, B., Liu, H.S., Shu, L.S., Jahn, B.M., Chung, S.L., Zhai, Y.Z., Liu, D.Y., 2014a. Early Neoproterozoic crustal evolution in northern Yili Block: insights from migmatite, orthogneiss and leucogranite of the Wenquan metamorphic complex in the NW Chinese Tianshan. Precambrian Res. 242, 58–81.
Wang, B., Shu, L.S., Liu, H.S., Gong, H.J., Ma, Y.Z., Mu, L.X., Zhong, L.L., 2014b. First evidence for ca. 780 Ma intra-plate magmatism and its implications for Neoproterozoic rifting of the North Yili Block and tectonic origin of the continental blocks in SW of Central Asia. Precambrian Res. 254, 258–272.
Wang, Q., Tang, G., Hao, L., Wyman, D., Ma, L., Dan, W., Zhang, X., Liu, J., Huang, T., Xu, C., 2020. Ridge subduction, magmatism, and metallogenesis. Sci. China Earth Sci. 63, 1499–1518.
Westbrook, G.K., Smith, M.J., 1983. Long decollements and mud volcanoes: evidence from the Barbados ridge complex for the role of high pore-water pressures in the development of an accretionary complex. Geology 11, 279–283.
Wilhem, C., Windley, B.F., Stampfli, G.M., 2012. The Altaids of Central Asia: a tectonic and evolutionary innovative review. Earth-Sci. Rev. 113, 303–341.
Winchester, J.A., Floyd, P.A., 1977. Geochemical discrimination of different magma series and their differentiation products using immobile elements. Chem. Geol. 20, 325–343.
Windley, B.F., Alexeiev, D., Xiao, W., Kröner, A., Badarch, G., 2007. Tectonic models for accretion of the Central Asian Orogenic Belt. J. Geol. Soc. London 164, 31–47.
Xiao, W., Santosh, M., 2014. The western Central Asian Orogenic Belt: a window to accretionary orogenesis and continental growth. Gondwana Res. 25, 1429–1444.

Xiao, W.J., Windley, B.F., Yuan, C., Sun, M., Han, C.M., Lin, S.F., Chen, H.L., Yan, Q.R., Liu, D.Y., Qin, K.Z., Li, J.L., Sun, S., 2009. Paleozoic multiple subduction–accretion processes of the southern Altaids. Am. J. Sci. 309, 221–270.

Xiao, W.J., Huang, B., Han, C., Sun, S., Li, J., 2010. A review of the western part of the Altaids: a key to understanding the architecture of accretionary orogens. Gondwana Res. 18, 253–273.

Xiao, W., Windley, B.F., Sun, S., Li, J., Huang, B., Han, C., Yuan, C., Sun, M., Chen, H., 2015. A tale of amalgamation of three Permo-Triassic Collage Systems in Central Asia: oroclines, sutures, and terminal accretion. Annu. Rev. Earth Planet. Sci. 43, 477–507.

Xiao, W., Windley, B.F., Han, C., Liu, W., Wan, B., Zhang, J., Ao, S., Zhang, Z., Song, D., 2017. Late Paleozoic to early Triassic multiple roll-back and oroclinal bending of the Mongolia collage in Central Asia. Earth Sci. Rev. 186, 94–128.

Xu, Z., Han, B.F., Ren, R., Zhou, Y.Z., Su, L., 2013. Palaeozoic multiphase magmatism at Barleik Mountain, southern West Junggar, Northwest China: implications for tectonic evolution of the West Junggar. Int. Geol. Rev. 55, 633–656.

Yakubchuk, A.S., 2004. Architecture and mineral deposit settings of the Altaid orogenic collage: a revised model. J. Asian Earth Sci. 23 (5), 761–779.

Yamamoto, K., 1987. Geochemical characteristics and depositional environments of cherts and associated rocks in the Franciscan and Shimanto terranes. Sediment. Geol. 52, 65–108.

Yarmolyuk, V.V., Kovach, V.P., Kozakov, I.K., Kozlovsky, A.M., Kotov, A.B., Rytsk, E.Y., 2012. Mechanisms of continental crust formation in the Central Asian Fold Belt. Geotectonics 46, 251–272.

Yarmolyuk, V.V., Kuz'min, M.I., Vorontsov, A.A., 2013. West pacific-type convergent boundaries and their role in the formation of the Central Asian Fold Belt. Russ. Geol. Geophys. 54, 1427–1441.

Zhang, J., Xiao, W., Luo, J., Chen, Y., Windley, B.F., Song, D., Han, C., Safonova, I., 2018. Collision of the Tacheng block with the Mayile-Barleik-Tangbale accretionary complex in Western Junggar, NW China: implication for Early-Middle Paleozoic architecture of the western Altaids. J. Asian Earth Sci. 159, 259–278.

Zhen, Y.Z., Percival, I.G., 2003. Ordovician conodont biogeography – reconsidered. Lethaia 36 (4), 357–369.

Zheng, R.G., Zhao, L., Yang, Y.Q., 2019. Geochronology, geochemistry and tectonic implications of a new ophiolitic mélange in the northern West Junggar, NW China. Gondwana Res. 74, 237–250.

Zholtaev, G.Zh., Nikitina, O.I., Zhaimina, V.Ya., Seitmuratova, E.Yu., Pirogova, T.E., Ivanova, N.I., Fazylov, E.M., Musina, E.S., Nigmatova, S.A., Bayshashov, B.U., 2021. Decisions of the meeting on the unification of Phanerozoic Stratigraphic Schemes of Kazakhstan, Almaty, November 25-29, 2021. Explanatory note to the stratigraphic schemes developed and approved by the Meeting within the framework of the project "Modernization of stratigraphic schemes of the Phanerozoic of Kazakhstan based on the International chronostratigraphic chart - 2016-2021". Almaty, LLP «378», 236 p. (in Russian).

Zhu, Y., Chen, B., Qiu, T., 2015. Geology and geochemistry of the Baijiantan-Baikouquan ophiolitic mélanges: implications for geological evolution of West Junggar, Xinjiang, NW China. Geol. Mag. 152, 41–69.

Zhylkaidarov, A.M., 1998. Conodonts form Ordovician of Central Kazakhstan. Acta Palaeontol. Pol. 43, 53–68.

Zonenshain, L.P., Kuzmin, M.I., Natapov, L.M., 1990. Geology of the USSR: a plate tectonic synthesis. Geodynamic Monograph Series. Am. Geoph., Union, p. 328.

Zyabrev, S., Matsuoka, A., 1999. Late Jurassic (Tithonian) radiolarians from a clastic unit of the Khabarovsk complex (Russian Far East): significance for subduction accretion timing and terrane correlation. Isl. Arc 8, 30–37.